

## Spatiotemporal Dynamics of the Diffusive Mussel-Algae Model Near Turing-Hopf Bifurcation\*

Yongli Song<sup>†</sup>, Heping Jiang<sup>‡</sup>, Quan-Xing Liu<sup>§</sup>, and Yuan Yuan<sup>¶</sup>

**Abstract.** Intertidal mussels can self-organize into periodic spot, stripe, labyrinth, and gap patterns ranging from centimeter to meter scales. The leading mathematical explanations for these phenomena are the reaction-diffusion-advection model and the phase separation model. This paper continues the series studies on analytically understanding the existence of pattern solutions in the reaction-diffusion mussel-algae model. The stability of the positive constant steady state and the existence of Hopf and steady-state bifurcations are studied by analyzing the corresponding characteristic equation. Furthermore, we focus on the Turing-Hopf (TH) bifurcation and obtain the explicit dynamical classification in its neighborhood by calculating and investigating the normal form on the center manifold. Using theoretical and numerical simulations, we demonstrate that this TH interaction would significantly enhance the diversity of spatial patterns and trigger the alternative paths for the pattern development.

**Key words.** mussel-algae model, Turing-Hopf bifurcation, normal form, spatiotemporal dynamics

**AMS subject classifications.** 35B32, 35B35, 35B57, 92D40

**DOI.** 10.1137/16M1097560

**1. Introduction.** Since the seminal work by Turing [48], where a system of chemicals reacting with each other and diffusing across space could account for the main phenomena of morphogenesis in biology, the dynamics of spatial pattern formation has attracted many scholars, ranging from biologists [23, 25], physicists [5, 27], and ecologists [14, 26]. Over the past few decades, field survey and satellite images have revealed the spatial patterns in a wide variety of ecosystems where the underlying mechanism is ascribed to scale-dependent feedbacks [32]. Going beyond the application of spatial patterns in various ecosystems, pattern solutions also get a significant theoretical advance about their stability and dispersion behaviors [35–38]. Especially, the stability of positive steady state, the Hopf bifurcation of the steady state, and the Turing bifurcation have been extensively investigated in different

\*Received by the editors October 6, 2016; accepted for publication (in revised form) by Y. Nishivra May 19, 2017; published electronically November 2, 2017.

<http://www.siam.org/journals/siads/16-4/M109756.html>

**Funding:** This research is supported by the National Natural Science Foundations of China (Nos. 11571257, 11701208, and 41676084).

<sup>†</sup>Department of Mathematics, Hangzhou Normal University, Hangzhou 311121, China ([syl.mail@163.com](mailto:syl.mail@163.com)).

<sup>‡</sup>Department of Mathematics, Tongji University, Shanghai, 200092, China ([jiangheping@hsu.edu.cn](mailto:jiangheping@hsu.edu.cn)).

<sup>§</sup>State Key Laboratory of Estuarine and Coastal Research, East China Normal University, Shanghai 200062, China ([qxliu@sklec.ecnu.edu.cn](mailto:qxliu@sklec.ecnu.edu.cn)).

<sup>¶</sup>Department of Mathematics and Statistics, Memorial University of Newfoundland, St. John's, Newfoundland, A1C 5S7, Canada ([yyuan@mun.ca](mailto:yyuan@mun.ca)).

reaction-diffusion systems [1–4, 10–12, 16, 22, 24, 28–30, 33, 34, 43–47, 51, 53–61]. Although there are plenty of models existing the Turing-Hopf bifurcation region but their dynamical properties are rarely understood in theory.

As well as implication of the mussel bed patterns, van de Koppel et al. [50] present a simple mathematical model that unravels their patterning formation process. For mussel bed ecosystems, the algae are the main food source for mussels, and the advection of algae is assumed to be constant, directed from the open sea toward the shore. In the intertidal flat, mussel beds are subject to disruption by predation, wave action, and ice scouring [7]. Van de Koppel's [50] model includes a positive feedback to describe these facilitated effects at higher mussel densities. Hitherto, many ecologists and mathematicians have focused on mussel bed development with mussel-algae models [3, 12, 17–21, 52], in which the theoretical studies suggest that self-organized patterns would affect the emergent properties of ecosystems in large-scale space [50]. Based on nonlinear numerical continue approaches, Wang et al. [52] have found that spatial patterns would exist at a remarkably lower food concentration compared with the classic linear stability, which explores the validity of predicting the pattern existence near the tipping point. Ghazaryan and Manukian [12] have applied geometric singular perturbation theory to analyze the nonlinear mechanisms of pattern wave formation on mussel-algae interaction with the tidal flow.

For the Turing-Hopf (TH) bifurcation, which is codimension-two bifurcation, periodic oscillations occur both spatially and temporally. Much previous work has focused on TH bifurcations of predator-prey-type reaction-diffusion systems and displaying the rich dynamics near the bifurcation point (see [2, 24, 33, 34] and references therein), most of which are based on the numerical results but lack rigorous theoretical analysis for the rich dynamics near the TH bifurcation point. However, Song et al. [46, 47] have verified the rigorous mathematical analysis and simulated the rich dynamics near the bifurcation point. The classification of the spatiotemporal dynamics in a neighborhood of the bifurcation point can be figured out in the framework of the normal forms. Motivated by the work of [46, 47], we study the TH bifurcation for the diffusive mussel-algae model with the Neumann boundary condition in one-dimensional spatial domain. Compared with the work done in [46, 47], this article has three innovations: first, we calculate the quadratic approximation of parameters of normal form such that the dynamical domain of the TH bifurcation can be divided more accurately; second, we take the diffusion coefficient as one of bifurcation parameters of TH bifurcation, which reflect the effect of the diffusion coefficient on the dynamical behavior of the original system; third, we apply the theoretical results to a real mussel-algae model and provide some interesting pattern formations.

The rest of this article is organized as follows. In section 2, after investigating the stability of the positive steady state and occurrence of Hopf bifurcation of the local system, we study the existence of the Hopf bifurcation and steady-state bifurcation for the diffusive mussel-algae model, then the TH bifurcation point is followed. In section 3, we derive the normal form of TH bifurcation for a general partial differential equation with two bifurcation parameters, one of them relating to the diffusion parameter, and discuss the dynamical behavior near the TH bifurcation point. In section 4, some numerical simulations are presented to illustrate and expand our theoretical results. Finally, we end this paper with some discussions on its ecological implications in section 5.

**2. Dynamics in a diffusive mussel-algae model.** Cangelosi et al. [3] have modified the unidirectional advection formulation of algal concentration into a random Brownian dispersion that obtained similar Turing patterns for the original mussel-algae model by employing weakly nonlinear diffusive instability analysis:

$$(2.1) \quad \begin{cases} \frac{\partial M}{\partial s} = ecAM - d_M \frac{k_M}{k_M + M} M + D_M \Delta M, \\ \frac{\partial A}{\partial s} = (A_{UP} - A)\rho - \frac{c}{H} AM - V \frac{\partial A}{\partial X} + D_A \Delta A, \end{cases}$$

where  $M$  is the density of mussel,  $A$  is the density of algae,  $\Delta = \frac{\partial^2}{\partial X^2} + \frac{\partial^2}{\partial Y^2}$ ,  $e$  is a conversion constant relating ingested algae to mussel biomass production,  $c$  is the consumption constant,  $d_M$  is the maximal per capita mussel mortality rate,  $k_M$  is the saturation rate of mussel,  $A_{UP}$  describes the uniform concentration of algae in the upper reservoir water layer,  $\rho$  is the exchanging rate between the lower and upper water layers,  $H$  is the height of the lower water layer,  $V$  is the speed of the tidal current assumed to be acting in the positive  $X$ -direction, and  $D_M$  and  $D_A$  are the motility and lateral diffusion coefficients of the mussel and algae, respectively.

Following [3] and introducing the dimensionless variables and parameters by

$$(x, y) = (X, Y) \sqrt{\frac{\omega}{D_A}}, t = d_M s, m = \frac{M}{k_M}, a = \frac{A}{A_{UP}},$$

with  $\omega = \frac{ck_M}{H}$ , and

$$r = \frac{ecA_{UP}}{d_M}, \alpha = \frac{\rho}{\omega}, \gamma = \frac{d_M}{\omega}, \nu = \frac{V}{\sqrt{\omega D_A}}, \mu = \frac{D_M}{\gamma D_A},$$

system (2.1) can be transformed into

$$(2.2) \quad \begin{cases} \frac{\partial m}{\partial t} = rma - \frac{m}{1+m} + \mu \Delta m, \\ \gamma \frac{\partial a}{\partial t} = \alpha(1-a) - ma - \nu \frac{\partial a}{\partial x} + \Delta a. \end{cases}$$

Note that although algae are thought of as advection with tidal flow at large scale, they actually disperse as Brownian particles in the fluid at small-scale space. The lab experiment revealed that mussels can actively move both within and between clusters [17, 49], which means that the influence of the advection with tidal flow at small-scale space on the mussel bed is very small. When  $\nu = 0$  and  $\gamma$  is sufficiently small, Cangelosi et al. [3] investigated the spatial patterns of system (2.2) on an unbounded planar spatial domain by employing weakly nonlinear diffusive instability analysis, and the main result is that several kinds of periodic mussel bed patterns are predicted, such as rhombic, hexagonal arrays, and isolated clusters of clumps or gaps.

Although advection and diffusion are two different ecological processes, in real mussel bed ecosystems, these processes normally coexist and share the same activator-inhibitor mechanism [21]. For the emergent properties of spatial self-organization patterns, the advection and diffusion are equivalent. Therefore, we revisit (2.2) in the case of no advection and with one-dimensional spatial variable  $x$  subject to Neumann boundary condition. We are interested

in the spatiotemporal dynamics near the TH bifurcation point. More specifically, we consider (2.2) with Neumann boundary condition in the domain  $[0, l\pi]$  and certain initial conditions as the following reaction-diffusion system:

$$(2.3) \quad \begin{cases} \frac{\partial m}{\partial t} = rma - \frac{m}{1+m} + \mu m_{xx}, \\ \gamma \frac{\partial a}{\partial t} = \alpha(1-a) - ma + a_{xx}, \\ m_x(0, t) = m_x(l\pi, t) = a_x(0, t) = a_x(l\pi, t) = 0, t \geq 0, \\ m(x, t) = \phi(x, t), a(x, t) = \psi(x, t) \geq 0, x \in [0, l\pi]. \end{cases}$$

It is easy to check that system (2.3) has a boundary steady state  $E_0(0, 1)$  and a positive steady state  $E^*(\frac{\alpha(r-1)}{1-\alpha r}, \frac{1-\alpha r}{r(1-\alpha)})$  provided that

$$(H1) \ 0 < \alpha^{-1} < r < 1, \text{ or } (H2) \ 0 < \alpha < r^{-1} < 1.$$

**2.1. Stability and bifurcation analysis for the nonspatial system.** We first discuss the dynamics of the following nonspatial system:

$$(2.4) \quad \begin{cases} \frac{dm}{dt} = rma - \frac{m}{1+m}, \\ \gamma \frac{da}{dt} = \alpha(1-a) - ma. \end{cases}$$

The linearization of (2.4) is

$$\begin{pmatrix} \frac{dm(t)}{dt} \\ \frac{da(t)}{dt} \end{pmatrix} = \begin{pmatrix} b_{11} & b_{12} \\ b_{21} & b_{22} \end{pmatrix} \begin{pmatrix} m(t) \\ a(t) \end{pmatrix}.$$

The characteristic equation is

$$(2.5) \quad \lambda^2 + T_0\lambda + J_0 = 0,$$

where

$$T_0 = -(b_{11} + b_{22}), \quad J_0 = b_{11}b_{22} - b_{12}b_{21}.$$

For the boundary steady state  $E_0$ , we have

$$b_{11} = r - 1, \quad b_{12} = 0, \quad b_{21} = -\frac{1}{\gamma}, \quad b_{22} = -\frac{\alpha}{\gamma},$$

and then

$$T_0 = 1 - r + \frac{\alpha}{\gamma}, \quad J_0 = -\frac{\alpha(r-1)}{\gamma},$$

which means that the boundary steady state  $E_0$  is stable for  $r < 1$  and unstable for  $r > 1$ .

For the positive steady state  $E^*$ , we have

$$(2.6) \quad b_{11} = \frac{(1-\alpha r)\alpha(r-1)}{(1-\alpha)^2}, \quad b_{12} = \frac{\alpha r(r-1)}{1-\alpha r}, \quad b_{21} = -\frac{1}{\gamma} \frac{1-\alpha r}{r(1-\alpha)}, \quad b_{22} = -\frac{1}{\gamma} \frac{\alpha r(1-\alpha)}{(1-\alpha r)},$$

and

$$(2.7) \quad T_0 = -\frac{(1-\alpha r)\alpha(r-1)}{(1-\alpha)^2} + \frac{1}{\gamma} \frac{\alpha r(1-\alpha)}{1-\alpha r}, \quad J_0 = \frac{1}{\gamma} \frac{\alpha(r-1)(1-\alpha r)}{1-\alpha}.$$

It follows that the positive steady state  $E^*$  is unstable when the condition (H1) holds because  $J_0 < 0$  under this condition. If (H2) holds, then  $J_0 > 0$ . Thus, the positive steady state  $E^*$  is asymptotically stable when  $T_0 > 0$  and unstable when  $T_0 < 0$ . Obviously,  $\gamma$  does not affect the existence of the positive steady state  $E^*$  but does affect its stability. In what follows, we investigate the effect of  $\gamma$  on the stability of positive steady state  $E^*$ . Solving  $T_0 = 0$  for  $\gamma$ , we have

$$(2.8) \quad \gamma = \gamma(r, \alpha) \triangleq \frac{r(1-\alpha)^3}{(1-\alpha r)^2(r-1)},$$

and we have the following results on the stability and Hopf bifurcation of the positive steady state  $E^*$  of system (2.4).

**Theorem 2.1.** *Assume that the condition (H<sub>2</sub>) holds and  $\gamma(r, \alpha)$  is determined by (2.8).*

- (i) *The positive steady state  $E^*$  of system (2.4) is stable for  $\gamma < \gamma(r, \alpha)$  and unstable for  $\gamma > \gamma(r, \alpha)$*
- (ii) *For fixed  $\alpha$  and  $\gamma > \gamma_{min}^*$ , system (2.4) undergoes Hopf bifurcations at  $r = r_j, j = 1, 2$ , where  $\gamma_{min}^*$  is determined by (2.9) and  $r_1$  and  $r_2$  are two roots of equation (2.8) with respect to  $\alpha$  and  $\gamma$ .*

*Proof.*

(i) From the condition (H<sub>2</sub>), it is easy to verify that  $J_0 > 0$  and  $T_0 > 0$  for  $\gamma < \gamma(r, \alpha)$  and  $T_0 < 0$  for  $\gamma > \gamma(r, \alpha)$ . Thus, two roots of the characteristic equation (2.5) with (2.6) and (2.7) has negative real parts if and only if  $\gamma < \gamma(r, \alpha)$ . This completes the proof of (i).

(ii) It follows from (2.8) that

$$\gamma_r = \frac{(1-\alpha)^3(2\alpha r^2 - \alpha r - 1)}{(1-\alpha r)^3(r-1)^2},$$

which implies that when (H<sub>2</sub>) holds,  $\gamma_r < 0$  for  $r < r_*$  and  $\gamma_r > 0$  for  $r > r_*$ , where

$$r_* = \frac{\alpha + \sqrt{\alpha^2 + 8\alpha}}{4\alpha}.$$

Thus, for fixed  $\alpha$ , the function  $\gamma = \gamma(r, \alpha)$  is decreasing for  $r < r_*$  and increasing  $r > r_*$  with respect to the variable  $r$ , and when  $r = r_*$ , the function  $\gamma = \gamma(r, \alpha)$  reaches its minimal value

$$(2.9) \quad \gamma_{min}^* \triangleq \gamma(\alpha, r_*) = \frac{16(\alpha + \sqrt{\alpha^2 + 8\alpha})(1-\alpha)^3}{(4-\alpha - \sqrt{\alpha^2 + 8\alpha})(\sqrt{\alpha^2 + 8\alpha} - 3\alpha)}.$$

Therefore, for fixed  $\alpha$  and  $\gamma > \gamma_{min}^*$ , equation (2.8) has two roots  $r = r_1$  and  $r = r_2$  with  $r_1 < r_* < r_2$ , at which the characteristic equation (2.5) has a pair of purely imaginary roots  $\pm i\sqrt{J_{01}}$  and  $\pm i\sqrt{J_{02}}$ , respectively, where

$$J_{0j} = \frac{1}{\gamma} \frac{\alpha(r_j - 1)(1 - \alpha r_j)}{1 - \alpha}, \quad j = 1, 2.$$

Taking  $r$  as a parameter, considering  $T_0$  and  $J_0$  as functions of  $r$ , and letting  $\lambda(r) = \beta(r) + i\omega(r)$  be the root of (2.5) satisfying  $\beta(r_j) = 0, \omega(r_j) = \sqrt{J_0}$ , then, by (2.5), (2.6), and (2.7), we have

$$\beta'(r_j) = -\frac{1}{2}T_0'(r_j) = -\frac{1}{2} \frac{\alpha(2\alpha r_j^2 - \alpha r_j - 1)}{r_j(1 - \alpha)^2},$$

where we have used  $T_0(r_j) = 0$ . In addition, noticing that  $r_1 < r_* < r_2$  and  $2\alpha r_*^2 - \alpha r_* - 1 = 0$ , we obtain

$$\beta'(r_1) > 0, \beta'(r_2) < 0,$$

which, together with the fact that the characteristic equation (2.5) has a pair of purely imaginary roots  $\pm i\sqrt{J_0}$  at  $r_j$ , implies that system (2.4) undergoes Hopf bifurcations at  $r = r_j, j = 1, 2$ . ■

The existence of the positive steady state  $E^*$  of system (2.4) is shown in the regions of  $R_1$  and  $R_2$  in Figure 1(A), which are independent of the value of  $\gamma$ , whereas the positive steady state  $E^*$  is unstable in  $R_1$  for any  $\gamma$  and might be stable in  $R_2$  depending on the choice of  $\gamma$ . By fixing the value of  $\alpha$ , the stability and instability regions related to the parameters  $r$  and  $\gamma$  are given in Figure 1(B).

**2.2. Stability, Turing instability, and TH bifurcation for the diffusive system.** In this subsection, we proceed to consider the diffusive mussel-algae model (2.3). The positive equilibrium  $E^*$  for the local model (2.4) is a spatially homogeneous steady state for the reaction-diffusion model (2.3). We investigate the diffusion-driven instability and the spatio-temporal dynamics for this steady state  $E^*$  under the condition  $(H_2)$ . The linearization of (2.3) at  $E^*$  is

$$(2.10) \quad \begin{pmatrix} \frac{\partial m(t)}{\partial t} \\ \frac{\partial a(t)}{\partial t} \end{pmatrix} = D\Delta \begin{pmatrix} m(t) \\ a(t) \end{pmatrix} + A \begin{pmatrix} m(t) \\ a(t) \end{pmatrix},$$

where

$$D\Delta = \begin{pmatrix} \mu \frac{\partial^2}{\partial x^2} & 0 \\ 0 & \frac{1}{\gamma} \frac{\partial^2}{\partial x^2} \end{pmatrix}, \quad A = \begin{pmatrix} b_{11} & b_{12} \\ b_{21} & b_{22} \end{pmatrix},$$

and  $b_{ij}$  is the same as in (2.6).

The characteristic equation of (2.10) subject to the Neumann boundary condition is

$$(2.11) \quad \Delta_k = \lambda^2 + T_k\lambda + J_k = 0, \quad k \in \mathbb{N}_0,$$

where  $\mathbb{N}_0$  is the set of nonnegative integers,  $k$  is identified as the wave number, and

$$(2.12) \quad T_k = \left(\mu + \frac{1}{\gamma}\right) \frac{k^2}{l^2} + T_0, \quad J_k = \frac{\mu k^4}{\gamma l^4} - \left(\mu b_{22} + \frac{1}{\gamma} b_{11}\right) \frac{k^2}{l^2} + J_0,$$

with  $T_0$  and  $J_0$  being defined by (2.7).

It is well known that the positive steady state  $E^*$  of (2.3) is locally asymptotically stable if and only if all roots of the characteristic equation (2.11) have negative real parts, i.e.,  $T_k > 0$  and  $J_k > 0$  for all  $k \in \mathbb{N}_0$ , and the bifurcation may occur when it is not satisfied. Specifically, around the positive steady state  $E^*$ , we have the following results.

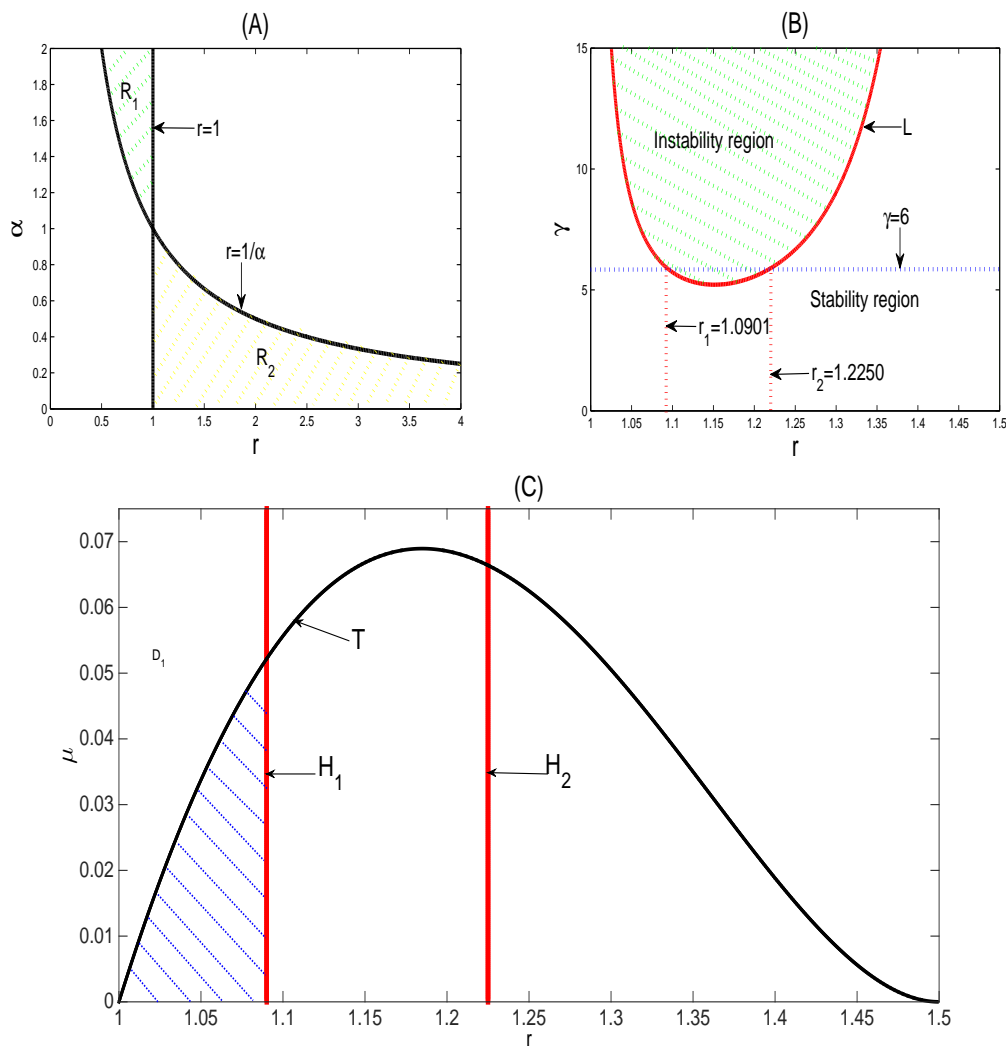


**Figure 1.** (A): The positive steady state  $E^*$  in (2.4) exists in the regions  $R_1$  and  $R_2$  but is unstable in  $R_1$  and is possible stable in  $R_2$  which depends on the choice of  $\gamma$ . (B): Stability/instability regions for the positive steady state  $E^*$  with  $\alpha = \frac{2}{3}$  in the  $r - \gamma$  plane. The curve marked by  $L$  is the Hopf bifurcation curve. (C): Bifurcation diagram for the diffusive mussel-algae model (2.3) with  $\alpha = \frac{2}{3}, \gamma = 6$  in the  $r - \mu$  plane. The curves marked by  $H_1$  and  $H_2$  are Hopf bifurcation curves, and the curve marked by  $T$  is the Turing bifurcation curve. The shadow region between two curves  $T$  and  $H_1$  is the Turing instability region.

**Theorem 2.2.** If the condition  $(H_2)$  holds, then when  $0 < \gamma < \gamma_{min}^*$ , there is no Hopf bifurcation for the diffusive mussel-algae model (2.3).

*Proof.* From Theorem 2.1 and the definition  $\gamma_{min}^*$  in (2.9), it follows that if the condition  $(H_2)$  holds and  $0 < \gamma < \gamma_{min}^*$ , then  $T_0 > 0$ . This, together with (2.12), leads to  $T_k > 0$  for any  $\mu > 0$  and  $k \in \mathbb{N}_0$ . So, the Hopf bifurcation cannot occur for the diffusive mussel-algae model (2.3) in this case. ■

If in the absence of diffusion the positive steady state  $E^*$  is stable under certain condition but becomes unstable because of the existence of diffusion, we call this instability the diffusion-driven Turing instability. Thus, diffusion-driven Turing instability occurs only when there exists at least one positive integer  $k$  such that  $J_k < 0$ .

**Theorem 2.3.** *If the condition  $(H_2)$  holds and  $\gamma < \gamma(r, \alpha)$ , then when  $\mu \geq \mu_*$ , there is no diffusion-driven Turing instability, where*

$$\mu_* = \frac{(r - 1)(1 - \alpha r)^2}{r(1 - \alpha)^3}.$$

*Proof.* It is easy from (2.12) to verify that  $\mu b_{22} + \frac{1}{\gamma} b_{11} \leq 0$  if and only if  $\mu \geq \mu_*$ . In addition, notice that  $J_0 > 0$ . Thus, if  $\mu \geq \mu_*$ , then  $J_k > 0$  for any  $k \in \mathbb{N}_0$ . ■

**Theorem 2.4.** *If the condition  $(H_2)$  holds, then for the diffusive mussel-algae model (2.3), we have the following:*

- (i) *when  $0 < \gamma < \gamma_{min}^*$ , the boundary of stability region in the  $r - \mu$  plane consists of the critical Turing bifurcation curve  $\mu = \mu(r, k_*^2)$ , and there is no TH bifurcation;*
- (ii) *when  $\gamma > \gamma_{min}^*$ , the boundary of stability region in the  $r - \mu$  plane consists of Hopf bifurcation curves  $H_j$  determined by  $r = r_j, j = 1, 2$ , and the critical Turing bifurcation curve  $\mu = \mu(r, k_*^2)$ , and TH bifurcation can occur at the interaction points  $(r_j, \mu^*)$  with  $\mu^* = \mu(r_j, k_*^2)$ , where  $\mu(r_j, k_*^2)$  is determined by (2.13) and  $k_*$  is determined by (2.15) and (2.16).*

*Proof.* First, we analyze the existence of Turing bifurcation. Solving  $J_k = 0$  determined by (2.12) for  $\mu$ , we obtain

$$(2.13) \quad \mu = \mu(r, k^2) \triangleq A_1 \frac{k^2 - A_2}{k^2(k^2 + A_3)},$$

where for  $0 < \alpha < 1$  and  $1 < r < \frac{1}{\alpha}$ ,

$$A_1 = \frac{l^2(1 - \alpha r)\alpha(r - 1)}{(1 - \alpha)^2} > 0, \quad A_2 = l^2(1 - \alpha) > 0, \quad A_3 = \frac{l^2\alpha r(1 - \alpha)}{1 - \alpha r} > 0.$$

It follows from (2.13) that  $\mu(r, k^2) > 0$  if and only if  $k > l\sqrt{1 - \alpha}$ . Further, we have

$$\mu(1, k^2) = \mu\left(\frac{1}{\alpha}, k^2\right) = 0$$

and

$$\begin{aligned} \mu_r(r, k^2) &= \frac{l^2\alpha(k^2 - A_2)}{k^2(1 - \alpha)^2(k^2 + A_3)(k^2(1 - \alpha r) + l^2\alpha r(1 - \alpha))} (k^2(1 - \alpha r)(1 + \alpha - 2\alpha r) + l^2\alpha(1 - \alpha)(\alpha r - 2\alpha r^2 + 1)) \\ &= \frac{l^2\alpha(k^2 - A_2)}{k^2(1 - \alpha)^2(k^2 + A_3)(k^2(1 - \alpha r) + l^2\alpha r(1 - \alpha))} (Q_1 r^2 + Q_2 r + Q_3), \end{aligned}$$

where

$$Q_1 = 2\alpha^2(k^2 - l^2(1 - \alpha)), \quad Q_2 = l^2\alpha^2(1 - \alpha) - k^2\alpha(3 + \alpha), \quad Q_3 = k^2(1 + \alpha) + l^2\alpha(1 - \alpha).$$

Noticing that  $Q_1 > 0$  for  $k > l\sqrt{1-\alpha}$ ,  $Q_3 > 0$ , and for  $1 < r < \frac{1}{\alpha}$

$$\mu_r(1, k^2) = \frac{l^2\alpha(k^2 - l^2(1-\alpha))}{k^2(k^2 + l^2\alpha)}(1-\alpha) > 0, \quad \mu_r\left(\frac{1}{\alpha}, k^2\right) = \frac{2l^2\alpha(k^2 - A_2)(1-r)}{k^2r(1-\alpha)^2(k^2 + A_3)} < 0,$$

we have

$$(2.14) \quad \mu_r(r, k^2) \begin{cases} > 0, & 1 < r < r^*, \\ < 0, & r^* < r < \frac{1}{\alpha}, \end{cases}$$

where

$$r^* = \frac{-Q_2 - \sqrt{Q_2^2 - 4Q_1Q_3}}{2Q_1}$$

due to  $\mu_r(r, k^2) > 0$  for sufficiently large  $r$ . It follows from (2.14) that for fixed  $k$ , the function  $\mu = \mu(r, k^2)$  is increasing for  $1 < r < r^*$  and decreasing for  $r^* < r < \frac{1}{\alpha}$  and obtain its maximum at  $r = r^*$ .

Assume that  $z = k^2$ ; then  $\mu(r, z) = A_1 \frac{z-A_2}{z(z+A_3)}$ . Differentiating  $\mu(r, z)$  with respect to  $z$  yields

$$\mu_z(r, z) = \frac{-A_1((z-A_2)^2 - A_2^2 - A_2A_3)}{z^2(z+A_3)^2} \begin{cases} > 0, & 0 < z < z_*, \\ < 0, & z > z_*, \end{cases}$$

where

$$z_* = A_2 + \sqrt{A_2(A_2 + A_3)} = l^2(1-\alpha) \left(1 + \frac{1}{\sqrt{1-\alpha r}}\right).$$

The function  $\mu(r, z)$  reaches its maximum at  $z = z_*$  for  $z > 0$  and fixed  $r$ . Therefore, the function  $\mu(r, k^2)$  reaches its maximum at  $k = k_*$  for fixed  $r$  and  $k \in \mathbb{N} = \{1, 2, \dots\}$  with

$$(2.15) \quad k_* = \begin{cases} k_0, & \text{if } \mu(r, k_0^2) \geq \mu(r, (k_0+1)^2), \\ k_0+1, & \text{if } \mu(r, k_0^2) < \mu(r, (k_0+1)^2), \end{cases}$$

where

$$(2.16) \quad k_0 = \left[ l\sqrt{(1-\alpha) \left(1 + \frac{1}{\sqrt{1-\alpha r}}\right)} \right],$$

where  $[\cdot]$  is the integer part function.

In addition, it follows from Theorem 2.1 that when  $0 < \gamma < \gamma_{min}^*$ , there is no Hopf bifurcation for the diffusive mussel-algae model (2.3). This, together with the above discussions on Turing bifurcation, confirms conclusion (i).

For fixed  $\gamma$  and  $\gamma > \gamma_{min}^*$ , we also have that  $T_0 > 0$  for  $r < r_1$  or  $r > r_2$  and  $T_0 < 0$  for  $r_1 < r < r_2$ . Thus, there is no Hopf bifurcation for  $r < r_1$  or  $r > r_2$  in the  $r - \mu$  plane. So,  $r = r_1$  and  $r = r_2$  are two critical Hopf bifurcation curves. This, together with the above discussions on Turing bifurcation and Theorem 2.1, completes the proof of conclusion (ii). ■

In order to investigate the influence of the diffusion coefficient  $\mu$  on the spatiotemporal patterns, we fix the parameter values  $l, \alpha, \gamma$  for numerical simulations and consider  $r$  and  $\mu$  as bifurcation parameters. For  $l = 10, \alpha = \frac{2}{3}$ , from (2.9) we have  $\gamma_{min}^* \doteq 5.2151$ . If we take  $\gamma < \gamma_{min}^*$ , by Theorem 2.2, there is no Hopf bifurcation. Since we are interested in the interaction of Turing bifurcation and Hopf bifurcation, we consider only the case  $\gamma > \gamma_{min}^*$ . Taking  $\gamma = 6 > \gamma_{min}^*$ , by (2.8) and Theorem 2.1, we have the Hopf bifurcation points  $r_1 \doteq 1.0901, r_2 \doteq 1.2250$ , as shown in Figure 1(B). It follows from (2.16) that  $k_0 = 10$  when  $r < 1.2831$ . So, the critical Turing bifurcation curve is one of  $J_{10} = 0$  and  $J_{11} = 0$ . Furthermore, a calculation shows that  $\mu(r, 10^2) > \mu(r, 11^2)$  for  $1 < r < 1.2148$  and  $\mu(r, 10^2) \leq \mu(r, 11^2)$  for  $1.2148 \leq r < 1.2831$ . So, we have  $k_* = 10$  for  $1 < r < 1.2148$  and  $k_* = 11$  for  $1.2148 \leq r < 1.2831$ . Thus, the critical Turing bifurcation curves are defined by  $J_{10} = 0$  for  $r < 1.2148$  and by  $J_{11} = 0$  for  $1.2148 \leq r < 1.2831$ . The Turing bifurcation curve defined by  $J_{10} = 0$  interacts with the Hopf bifurcation curve  $r = r_1$  at  $(r, \mu) = (1.0901, 0.0522)$ , and the Turing bifurcation curve defined by  $J_{11} = 0$  interacts with the Hopf bifurcation curve  $r = r_2$  at  $(r, \mu) = (1.2250, 0.0665)$ . These two points are TH bifurcation points. Since the theoretical analysis near these two points are similar, we consider only the TH bifurcation point  $(r, \mu) = (r_1, \mu^*)$  with  $r_1 = 1.0901, \mu^* = 0.0522$ .

We draw all these particular curves in Figure 1(C), where the solid black curve ( $T$ ) represents the occurrence of Turing bifurcation defined by  $J_0 = 10$  and the solid red vertical lines  $H_1$  and  $H_2$  represent the occurrence of two Hopf bifurcations. These curves divide the plane into several regions where in  $D_1$ , the positive steady state is asymptotically stable and the shadow region is the Turing instability region.

What kinds of dynamical behavior will the system present near the TH point  $(r_1, \mu^*)$ ? In the following, we are interested to find out the dynamical classification of system (2.3) near this bifurcation point.

### 3. Spatiotemporal dynamics of the diffusive mussel-algae model near the TH bifurcation point.

**3.1. Normal form of TH bifurcation for a general partial differential equations.** To study the spatiotemporal dynamics of a system in the neighborhood of TH bifurcation point, it is essential to obtain the normal form on the center manifold associated with codimension-2 TH bifurcation. Taking the effect of diffusion into account on the dynamical behavior and dividing the dynamical regions more precisely, we extend the work in [46, 47] and present the computation method of the normal form of TH bifurcation for a general reaction-diffusion equation subject to the Neumann boundary condition as follows.

Define the real-valued Sobolev space

$$X = \left\{ u \in (W^{2,2}(0, l\pi))^2, \frac{\partial u_i}{\partial x} = 0, x = 0, l\pi, i = 1, 2 \right\}$$

with the inner product

$$[u, v] = \sum_{i=1}^2 \int_0^{l\pi} u_i v_i dx, \text{ for } u = (u_1, u_2)^T, v = (v_1, v_2)^T \in X.$$

To investigate codimension-2 bifurcation in a system, we introduce two bifurcation parameters,  $\varepsilon_1$  and  $\varepsilon_2$ , and assume that Turing bifurcation occurs when  $\varepsilon_1 = 0$ , Hopf bifurcation occurs when  $\varepsilon_2 = 0$ , and consequently TH bifurcation occurs when  $\varepsilon_1 = \varepsilon_2 = 0$ . To explore the effect of diffusion coefficient, without loss of generality, we study the general reaction-diffusion system

$$(3.1) \quad u_t = d(\varepsilon_2)\Delta u + L(\varepsilon_1)u + F(u, \varepsilon_1), \quad x \in (0, l\pi), \quad t > 0,$$

with

$$u(t) = \begin{pmatrix} u_1(t) \\ u_2(t) \end{pmatrix}, \quad d(\varepsilon_2)\Delta = \begin{pmatrix} (d_1 + \varepsilon_2) \frac{\partial^2}{\partial x^2} & 0 \\ 0 & d_2 \frac{\partial^2}{\partial x^2} \end{pmatrix},$$

$$L(\varepsilon_1) = (l_{ij}(\varepsilon_1))_{2 \times 2}, \quad F(u, \varepsilon_1) = \begin{pmatrix} f^{(1)}(u, \varepsilon_1) \\ f^{(2)}(u, \varepsilon_1) \end{pmatrix},$$

and  $d_i > 0, i = 1, 2, \text{dom}(\Delta) \subset X, \varepsilon = (\varepsilon_1, \varepsilon_2) \in \mathbb{R}^2$ , and  $F : \mathbb{R}^2 \times \mathbb{R} \rightarrow \mathbb{R}^2$  are  $C^k (k \geq 3)$  with  $F(0, \varepsilon_1) = 0, D_1 F(0, \varepsilon_1) = 0$ .

In the following, we suppose that  $\varepsilon = 0$  is the bifurcation value and let  $L_0 = L(0)$ . System (3.1) can be transformed into the following system:

$$(3.2) \quad u_t = \mathcal{L}u + \tilde{F}(u, \varepsilon)$$

with

$$\mathcal{L}u = \begin{pmatrix} d_1 \frac{\partial^2}{\partial x^2} & 0 \\ 0 & d_2 \frac{\partial^2}{\partial x^2} \end{pmatrix} u + L_0 u$$

and

$$\begin{aligned} \tilde{F}(u, \varepsilon) &= \begin{pmatrix} \varepsilon_2 u_{1xx} \\ 0 \end{pmatrix} + L(\varepsilon_1)u - L_0 u + F(u, \varepsilon_1) \\ &= \begin{pmatrix} \varepsilon_2 \frac{\partial^2 u_1}{\partial x^2} \\ 0 \end{pmatrix} + \sum_{j_1+j_2+j_3 \geq 2} \frac{1}{j_1! j_2! j_3!} f_{j_1 j_2 j_3} u_1^{j_1} u_2^{j_2} \varepsilon_1^{j_3}, \quad f_{j_1 j_2 j_3} = \begin{pmatrix} f_{j_1 j_2 j_3}^{(1)} \\ f_{j_1 j_2 j_3}^{(2)} \end{pmatrix}. \end{aligned}$$

The eigenvalues of  $d\Delta$  are  $\delta_k^{(j)} = -d_j(\frac{k}{l})^2, k \in \mathbb{N}_0, j = 1, 2$ , and the corresponding normalized eigenfunctions is  $\beta_k^{(j)}$ , where

$$(3.3) \quad \beta_k^{(j)}(x) = \gamma_k(x)e_j, \quad \gamma_k(x) = \frac{\cos(\frac{kx}{l})}{\|\cos(\frac{kx}{l})\|_{2,2}} = \begin{cases} \frac{1}{\sqrt{l\pi}}, & \text{for } k = 0, \\ \sqrt{\frac{2}{l\pi}}\cos(\frac{kx}{l}), & \text{for } k \neq 0, \end{cases}$$

where  $e_j$  is the unit coordinate vector of  $\mathbb{R}^2$  and  $k$  is usually called wave number.

The characteristic equation associated with the linearized system of (3.2) is  $\prod_{k \in \mathbb{N}_0} \Gamma_k(\lambda) = 0$ , where  $\Gamma_k(\lambda) = \det(\mathcal{M}_k(\lambda))$  with  $\mathcal{M}_k(\lambda) = \text{diag}\{\lambda - \delta_k^{(1)}, \lambda - \delta_k^{(2)}\} - L_0$ . Assume that the equation  $\Gamma_0(\lambda) = 0$  has a pair of simple purely imaginary roots  $\pm i\omega$  and there exists an integer  $k_* \in \mathbb{N}$  such that the equation  $\Gamma_{k_*}(\lambda) = 0$  has a simple zero root  $\lambda = 0$ . Moreover, all the other roots of  $\prod_{k \in \mathbb{N}_0} \Gamma_k(\lambda) = 0$  have negative real parts.

For two vectors  $\varphi, \psi \in \mathbb{R}^2$ , denote their scalar product  $\langle \psi^T, \varphi \rangle = \psi^T \varphi$ . Let

$$\Phi_0 = (p_0, \overline{p_0}), \Phi_{k_*} = p_{k_*}, \Psi_0 = \text{col}(q_0^T, \overline{q_0^T}), \Psi_{k_*} = q_{k_*}^T,$$

where  $p_0 = (p_{01}, p_{02})^T \in \mathbb{C}^2$  and  $p_{k_*} = (p_{k_*1}, p_{k_*2})^T \in \mathbb{R}^2$  are the eigenvectors associated with the eigenvalues  $i\omega$  and  $0$ , respectively;  $q_0 = (q_{01}, q_{02})^T \in \mathbb{C}^2$  and  $q_{k_*} = (q_{k_*1}, q_{k_*2})^T \in \mathbb{R}^2$  are the corresponding adjoint eigenvectors; and  $\langle \Psi_0, \Phi_0 \rangle = I_2, \langle \Psi_{k_*}, \Phi_{k_*} \rangle = 1$ . Then  $u \in \mathcal{C}$  can be decomposed as

$$(3.4) \quad u = \left( \Phi_0 \begin{pmatrix} z_1 \\ z_2 \end{pmatrix} \right)^T \begin{pmatrix} \beta_0^{(1)} \\ \beta_0^{(2)} \end{pmatrix} + (\Phi_{k_*} z_3) \begin{pmatrix} \beta_{k_*}^{(1)} \\ \beta_{k_*}^{(2)} \end{pmatrix} + w \\ = (z_1 p_0 + z_2 \overline{p_0}) \gamma_0(x) + z_3 p_{k_*} \gamma_{k_*}(x) + \begin{pmatrix} w_1 \\ w_2 \end{pmatrix},$$

where  $z_1, z_2, z_3 \in \mathbb{R}, w \in X^s$ .

Let  $\Phi = \text{diag}\{\Phi_0, \Phi_{k_*}\}$  and  $z_x = (z_1 \gamma_0, z_2 \gamma_0, z_3 \gamma_{k_*})^T$ . Then  $u = \Phi z_x + w$ .  $B = \text{diag}\{i\omega, -i\omega, 0\}$  is a diagonal matrix, the operator  $M_j^1, j \geq 2$  defined in  $V_j^5(\mathbb{R}^3)$ , and we have a diagonal representation relative to the canonical basis  $\{z_1^{q_1} z_2^{q_2} z_3^{q_3} \varepsilon_1^{p_1} \varepsilon_2^{p_2} e_k, q_1, q_2, q_3, p_1, p_2 \in \mathbb{N}_0, q_1 + q_2 + q_3 + p_1 + p_2 = j\}$ , where  $e_k (k = 1, 2, 3)$  are unit vectors. It is easy to verify that

$$(3.5) \quad M_j^1(\varepsilon^p z^q e_\varsigma) Bz - B\varepsilon^p z^q e_\varsigma = i\omega (q_1 - q_2 + (-1)^\varsigma) \varepsilon^p z^q e_\varsigma, \\ M_j^1(\varepsilon^p z^q e_3) Bz - B\varepsilon^p z^q e_3 = i\omega (q_1 - q_2) \varepsilon^p z^q e_3,$$

where  $\varsigma = 1, 2$ . Then, from (3.5), we get

$$(3.6) \quad \text{Ker}(M_2^1) = \text{span}\{z_1 z_3 e_1, z_1 \varepsilon_1 e_1, z_1 \varepsilon_2 e_1, z_2 z_3 e_2, z_2 \varepsilon_1 e_2, z_2 \varepsilon_2 e_2, z_1 z_2 e_3, z_3^2 e_3, z_3 \varepsilon_1 e_3, z_3 \varepsilon_2 e_3, \\ \varepsilon_1 \varepsilon_2 e_3, \varepsilon_1^2 e_3, \varepsilon_2^2 e_3\}$$

and

$$(3.7) \quad \text{Ker}(M_3^1) = \text{span}\{z_1^2 z_2 e_1, z_1 z_3^2 e_1, z_1 z_3 \varepsilon_1 e_1, z_1 z_3 \varepsilon_2 e_1, z_1 \varepsilon_1^2 e_1, z_1 \varepsilon_2^2 e_1, z_1 \varepsilon_1 \varepsilon_2 e_1, z_1 z_2^2 e_2, z_2 z_3^2 e_2, \\ z_2 z_3 \varepsilon_1 e_2, z_2 z_3 \varepsilon_2 e_2, z_2 \varepsilon_1^2 e_2, z_2 \varepsilon_2^2 e_2, z_2 \varepsilon_1 \varepsilon_2 e_2, z_1 z_2 z_3 e_3, z_3^3 e_3, z_1 z_2 \varepsilon_1 e_3, \\ z_1 z_2 \varepsilon_2 e_3, z_3 \varepsilon_1^2 e_3, z_3 \varepsilon_2^2 e_3, z_3 \varepsilon_1 \varepsilon_2 e_3\}.$$

Following the results in [46, 47], we have the normal form for TH bifurcation as follows:

$$(3.8) \quad \dot{z} = Bz + \begin{pmatrix} (B_1^{(1)}\varepsilon_1 + B_1^{(2)}\varepsilon_2)z_1 \\ (B_2^{(1)}\varepsilon_1 + B_2^{(2)}\varepsilon_2)z_2 \\ (B_3^{(1)}\varepsilon_1 + B_3^{(2)}\varepsilon_2)z_3 \end{pmatrix} + \begin{pmatrix} B_{11}z_1^2z_2 + B_{12}z_1z_3^2 \\ B_{21}z_1z_2^2 + B_{22}z_2z_3^2 \\ B_{31}z_1z_2z_3 + B_{32}z_3^3 \end{pmatrix} + \begin{pmatrix} B_{13}z_1\varepsilon_1^2 + B_{14}z_1\varepsilon_2^2 + B_{15}z_1\varepsilon_1\varepsilon_2 \\ B_{23}z_2\varepsilon_1^2 + B_{24}z_2\varepsilon_2^2 + B_{25}z_2\varepsilon_1\varepsilon_2 \\ B_{33}z_3\varepsilon_1^2 + B_{34}z_3\varepsilon_2^2 + B_{35}z_3\varepsilon_1\varepsilon_2 \end{pmatrix} + h.o.t.,$$

where

$$B_{1j} = C_{1j} + \frac{3}{2}(D_{1j} + E_{1j}) = \overline{B_{2j}}, \quad B_{3j} = C_{3j} + \frac{3}{2}(D_{3j} + E_{3j}), \quad j = 1, 2, 3, 4, 5,$$

with the expression of  $B_{1j}, B_{2j}, B_{3j}$ ,  $j = 1, 2$  being the same as in [47] (see Appendix A). In this paper, we focus on finding the expression of  $B_i^{(1)}, B_i^{(2)}$ ,  $i = 1, 2, 3$  and  $B_{1j}, B_{2j}, B_{3j}$ ,  $j = 3, 4, 5$  (see Appendix B).

As for autonomous ODEs in the finite dimension space, by a recursive transformation of variables

$$(z, w) = (\tilde{z}, \tilde{w}) + \frac{1}{j!} (U_j^1(\tilde{z}, \varepsilon), U_j^2(\tilde{z}, \varepsilon)), \quad j \geq 2,$$

where  $U_j^1$  and  $U_j^2$  are homogeneous polynomials of degree  $j$  in  $\tilde{z}$  and  $\varepsilon$ . The normal form on the center manifold becomes

$$(3.9) \quad \dot{z} = Bz + \frac{1}{2!}g_2^1(z, 0, \varepsilon) + \frac{1}{3!}g_3^1(z, 0, \varepsilon) + O(|\varepsilon||z|^2),$$

where  $g_2^1$  and  $g_3^1$  are the second and third terms in  $(z, \varepsilon)$ , respectively, by dropping the tilde after each transformation of variable for simplification of notation.

The normal form (3.8) can be written in real coordinates  $\omega$  through the change of variables  $z_1 = v_1 - v_2i, z_2 = v_1 + v_2i, z_3 = v_3$ , and then in cylindrical coordinates by  $v_1 = \rho \cos \Theta, v_2 = \rho \sin \Theta, v_3 = s$ . Truncating at third-order terms and removing the azimuthal term, finally, (3.8) is equivalent to the following:

$$(3.10) \quad \begin{cases} \dot{\rho} = \nu_1(\varepsilon)\rho + \kappa_{11}\rho^3 + \kappa_{12}\rho s^2, \\ \dot{s} = \nu_2(\varepsilon)s + \kappa_{21}\rho^2s + \kappa_{22}s^3, \end{cases}$$

where

$$\begin{aligned} \nu_1(\varepsilon) &= \operatorname{Re} \left( B_1^{(1)}\varepsilon_1 + B_1^{(2)}\varepsilon_2 + B_{13}\varepsilon_1^2 + B_{14}\varepsilon_2^2 + B_{15}\varepsilon_1\varepsilon_2 \right), \\ \nu_2(\varepsilon) &= \operatorname{Re} \left( B_3^{(1)}\varepsilon_1 + B_3^{(2)}\varepsilon_2 + B_{33}\varepsilon_1^2 + B_{34}\varepsilon_2^2 + B_{35}\varepsilon_1\varepsilon_2 \right), \\ \kappa_{11} &= \operatorname{Re} (B_{11}), \quad \kappa_{12} = \operatorname{Re} (B_{12}), \quad \kappa_{21} = \operatorname{Re} (B_{31}), \quad \kappa_{22} = \operatorname{Re} (B_{32}). \end{aligned}$$

**3.2. Dynamical classification of the diffusive mussel-algae model near the TH bifurcation point.** In this subsection, we apply the theoretical results developed previously to the diffusive mussel-algae model to obtain the normal form of TH bifurcation; then we can classify the dynamics near the TH bifurcation point explicitly.

From Theorem 2.4 (ii) and Figure 1(C), when  $\alpha = 2/3, \gamma = 6$ , the point  $TH(r_1, \mu^*)$  with  $r_1 = 1.0901, \mu^* = 0.0522$  in the  $r - \mu$  plane is the TH bifurcation point of system (2.3). To apply the results in section 3.1, we set  $\varepsilon_1 = r - r_1, \varepsilon_2 = \mu - \mu^*, l = 10, k_* = 10$ , and rewrite the positive steady state as a parameter-dependent form  $E^*(m^*(\varepsilon_1), a^*(\varepsilon_1))$  with

$$m^*(\varepsilon_1) = \frac{\alpha(r_1 + \varepsilon_1 - 1)}{1 - \alpha(r_1 + \varepsilon_1)}, \quad a^*(\varepsilon_1) = \frac{1 - \alpha(r_1 + \varepsilon_1)}{(r_1 + \varepsilon_1)(1 - \alpha)}.$$

Setting  $\tilde{m}(x, t) = m(x, t) - m^*(\varepsilon_1), \tilde{a}(x, t) = a(x, t) - a^*(\varepsilon_1), \tilde{u}(x, t) = (\tilde{m}(x, t), \tilde{a}(x, t))^T$  and then dropping the tides for simplification of notation, the system (2.3) can be written as (3.2) with

$$u = \begin{pmatrix} m(x, t) \\ a(x, t) \end{pmatrix}, \quad \mathcal{L}u = \begin{pmatrix} \mu^* m_{xx} \\ \frac{1}{\gamma} a_{xx} \end{pmatrix} + L_0 u, \quad \tilde{F}(u, \varepsilon) = \begin{pmatrix} \varepsilon_2 m_{xx} \\ 0 \end{pmatrix} + F(u, \varepsilon_1),$$

where

$$L(\varepsilon_1) = \begin{pmatrix} b_{11}(\varepsilon_1) & b_{12}(\varepsilon_1) \\ b_{21}(\varepsilon_1) & b_{22}(\varepsilon_1) \end{pmatrix}, \quad L_0 = L(0), \quad F(u, \varepsilon_1) = \begin{pmatrix} f^{(1)}(u, \varepsilon_1) \\ f^{(2)}(u, \varepsilon_1) \end{pmatrix},$$

and  $b_{ij}(\varepsilon_1)$  is defined by (2.6) with  $r = r_1 + \varepsilon_1$ ,

$$f^{(1)}(m, a, \varepsilon_1) = (r_1 + \varepsilon_1)(m + m^*(\varepsilon_1))(a + a^*(\varepsilon_1)) - \frac{m + m^*(\varepsilon_1)}{1 + m + m^*(\varepsilon_1)},$$

$$f^{(2)}(m, a, \varepsilon_1) = \frac{\alpha}{\gamma}(1 - (a + a^*(\varepsilon_1))) - \frac{1}{\gamma}(m + m^*(\varepsilon_1))(a + a^*(\varepsilon_1)).$$

Let

$$\mathcal{M}_k = \begin{pmatrix} -\mu^* \frac{k^2}{l^2} + b_{11}(0) & b_{12}(0) \\ b_{21}(0) & -\frac{1}{\gamma} \frac{k^2}{l^2} + b_{22}(0) \end{pmatrix}.$$

It is easy to verify that  $\Phi_0 = (p_0, \bar{p}_0), \Phi_{k_*} = p_{k_*}, \Psi_0 = (q_0, \bar{q}_0)^T, \Psi_{k_*} = q_{k_*}$ , where

$$p_0 = \begin{pmatrix} p_{01} \\ p_{02} \end{pmatrix} = \begin{pmatrix} 1 \\ \frac{(i\omega_0(1-\alpha)^2 - (1-\alpha r_1)\alpha(r_1-1))(1-\alpha r_1)}{\alpha r_1(r_1-1)(1-\alpha)^2} \end{pmatrix},$$

$$q_0^T = (q_{01}, q_{02}) = \left( \frac{i\omega_0\gamma(1-\alpha r_1) + \alpha r_1(1-\alpha)}{2i\omega_0\gamma(1-\alpha r_1)}, \frac{\alpha r_1(r_1-1)}{2i\omega_0(1-\alpha r_1)} \right),$$

$$p_{k_*} = \begin{pmatrix} p_{k_*1} \\ p_{k_*2} \end{pmatrix} = \begin{pmatrix} 1 \\ \frac{(\mu^* \frac{k_*^2}{l^2} (1-\alpha)^2 - (1-\alpha r_1)\alpha(r_1-1))(1-\alpha r_1)}{\alpha r_1(r_1-1)(1-\alpha)^2} \end{pmatrix},$$

$$q_{k_*}^T = (q_{k_*1}, q_{k_*2}) = \left( \frac{\frac{k_*^2}{l^2} + \alpha r_1(1-\alpha)}{\gamma(1-\alpha r_1)T_{k_*}}, \frac{\alpha r_1(r_1-1)}{(1-\alpha r_1)T_{k_*}} \right),$$

with  $\omega_0 = \sqrt{\frac{1}{\gamma} \frac{\alpha(r_1-1)(1-\alpha r_1)}{1-\alpha}}$ .

By a direct computation, we obtain  $f_{020} = f_{210} = f_{120} = f_{030} = 0$ . Then, according to the procedure in section 3.1, the normal form truncated to the third-order terms is

$$(3.11) \quad \begin{cases} \dot{\rho} = (0.3917\varepsilon_1 - 2.6035\varepsilon_1^2)\rho - 0.0125624\rho^3 + 0.0045\rho s^2, \\ \dot{s} = (0.5309\varepsilon_1 - 1.4364\varepsilon_2 - 1.7079\varepsilon_1^2 - 2.8640\varepsilon_2^2 - 2.8627\varepsilon_1\varepsilon_2)s \\ \quad - 0.0236\rho^2 s - 0.0340s^3. \end{cases}$$

Notice that  $\rho \geq 0$  and  $s$  is arbitrarily real number. System (3.11) has a zero equilibrium  $A_0(0, 0)$  for all  $\varepsilon_1, \varepsilon_2$ , three possible boundary equilibria

$$A_1 \left( \sqrt{\frac{0.3917\varepsilon_1 - 2.6035\varepsilon_1^2}{0.0125}}, 0 \right),$$

$$A_2^\pm \left( 0, \pm \sqrt{\frac{0.5309\varepsilon_1 - 1.4364\varepsilon_2 - 1.7079\varepsilon_1^2 - 2.8640\varepsilon_2^2 - 2.8627\varepsilon_1\varepsilon_2}{0.0340}} \right),$$

and two possible positive equilibria  $A_3^\pm(\rho^*, \pm s^*)$ , where

$$\rho^* = \sqrt{\frac{0.1571\varepsilon_1 - 0.0646\varepsilon_2 - 0.9621\varepsilon_1^2 - 0.1289\varepsilon_2^2 - 0.1288\varepsilon_1\varepsilon_2}{0.0054}}$$

and

$$s^* = \sqrt{\frac{-(0.0260\varepsilon_1 + 0.1795\varepsilon_2 - 0.4009\varepsilon_1^2 + 0.3580\varepsilon_2^2 + 0.3578\varepsilon_1\varepsilon_2)}{0.0054}}.$$

From the existence and their stability of these five equilibria, we obtain the critical bifurcation lines as follows:

$$H : \varepsilon_1 = 0;$$

$$T : 0.5309\varepsilon_1 - 1.4364\varepsilon_2 - 1.7079\varepsilon_1^2 - 2.8640\varepsilon_2^2 - 2.8627\varepsilon_1\varepsilon_2 = 0;$$

$$T_1 : 0.1571\varepsilon_1 - 0.0646\varepsilon_2 - 0.9621\varepsilon_1^2 - 0.1289\varepsilon_2^2 - 0.1288\varepsilon_1\varepsilon_2 = 0, \varepsilon_1 < 0;$$

$$T_2 : 0.0260\varepsilon_1 + 0.1795\varepsilon_2 - 0.4009\varepsilon_1^2 + 0.3580\varepsilon_2^2 + 0.3578\varepsilon_1\varepsilon_2 = 0, \varepsilon_1 > 0.$$

Notice that the normal form (3.11) belongs to the so-called simple case described in [15]. Therefore, the bifurcation diagrams in the  $(\varepsilon_1, \varepsilon_2)$  parameter space and the corresponding phase portraits of the normal form system (3.11) plane can be shown in Figure 2. These four solid lines  $H, T, T_1$ , and  $T_2$  divide the  $(\varepsilon_1, \varepsilon_2)$  parameter plane into six regions with different dynamics.

According to the normal form theory of reaction-diffusion equations [9, 47], the dynamics of the normal form system (3.11) is topologically equivalent to the dynamics of the original diffusive system near the bifurcation point. In addition, notice that  $\varepsilon_1$  and  $\varepsilon_2$  are perturbation variables, respectively, of the original parameters  $r$  and  $\mu$  in the diffusive mussel-algae model system (2.3) at  $r = r_1, \mu = \mu^*$ . Thus, the dynamical classification of (2.3) near the TH bifurcation point  $TH(r_1, \mu^*)$  can be determined by the normal form system (3.11). By the procedure of the calculation of the normal form, it is easy to see that the equilibrium of



When  $(\varepsilon_1, \varepsilon_2) \in D_6$ , (3.11) has only one unstable zero equilibrium and two stable boundary equilibria  $A_2^+$  and  $A_2^-$  in the  $s$ -axis. This implies that the diffusive mussel-algae model (2.3) has three steady states: one is unstable and spatially homogeneous, and the other two are stable and spatially inhomogeneous.

We should address that the theory and method developed in this section is targeted at the dynamical behavior near a TH bifurcation point by obtaining the normal forms through the coordinate transformations and analyzing the dynamical information from the truncated normal forms. Once the conditions are determined for occurring TH bifurcation at the steady state, this method is valid, although only the local dynamical properties can be investigated.

### 3.3. Numerical simulations.

**3.3.1. The spatiotemporal dynamics near the TH bifurcation point.** According to the dynamics of the normal form system (3.11) and the bifurcation diagram Figure 2, the diffusive mussel-algae model (2.3) has four types of stable patterns: spatially homogeneous/inhomogeneous steady states and spatially homogeneous/inhomogeneous periodic solution. In the following, we use Matlab software to provide some simulated patterns.

Figure 3 shows the stable pattern in each region. For example, stable spatially homogeneous steady state exists in region  $D_1$ . Stable spatially inhomogeneous steady state exists in region  $D_6$ . Stable spatially homogeneous periodic solution exists in regions  $D_2$  and  $D_3$ . Stable spatially inhomogeneous solution exists in regions  $D_4$  and  $D_5$ . The numerical solutions suggest that mussel beds may disappear for short term when the environmental conditions are within the  $D_4$  and  $D_5$  regions. Hence, no collapse occurs for these ecosystems because they will rebuild quickly after a critical period. However, such transitory disappearance never occurs in classical Turing space.

In addition, there are three types of pattern transitions: (i) from unstable spatially inhomogeneous steady state to stable spatially homogeneous periodic solution, which exists in  $D_3$  (see Figure 4); (ii) from unstable spatially homogeneous periodic solution to stable spatially inhomogeneous periodic solution; and (iii) from unstable spatially inhomogeneous steady state to stable spatially inhomogeneous periodic solution. (ii) and (iii) occur in  $D_4$  (see Figures 5 and 6). In Figures 4–6, the first row (A–C) shows the dynamics of mussel, and the second row (D–F) depicts the dynamics of algae, while (A/D) presents the trends of the pattern transition, (B/E) gives the first part of the movement (transition), and (C/F) gives the final stable behavior. It is interesting to point that, with the same parameter  $(\varepsilon_1; \varepsilon_2) = (0.01; -0.003) \in D_4$  but different initial conditions, we can observe different pattern transitions but the same final patterns.

*Remark 3.1.* To emphasize our main contribution in calculating the higher-order terms, we would also like to mention that the coefficients of the terms  $\varepsilon_1^i \varepsilon_2^j \rho$  and  $\varepsilon_1^i \varepsilon_2^j s$  with  $i + j = 2$  are not calculated in [47], but it is necessary for the diffusive mussel-algae model (2.3) because the Turing bifurcation curve is different from a straight line. If we ignore these terms, the particular curves in the bifurcation diagram near the TH point become

$$\begin{aligned} H &: \varepsilon_1 = 0; \\ T^* &: 0.5309\varepsilon_1 - 1.4364\varepsilon_2 = 0; \end{aligned}$$

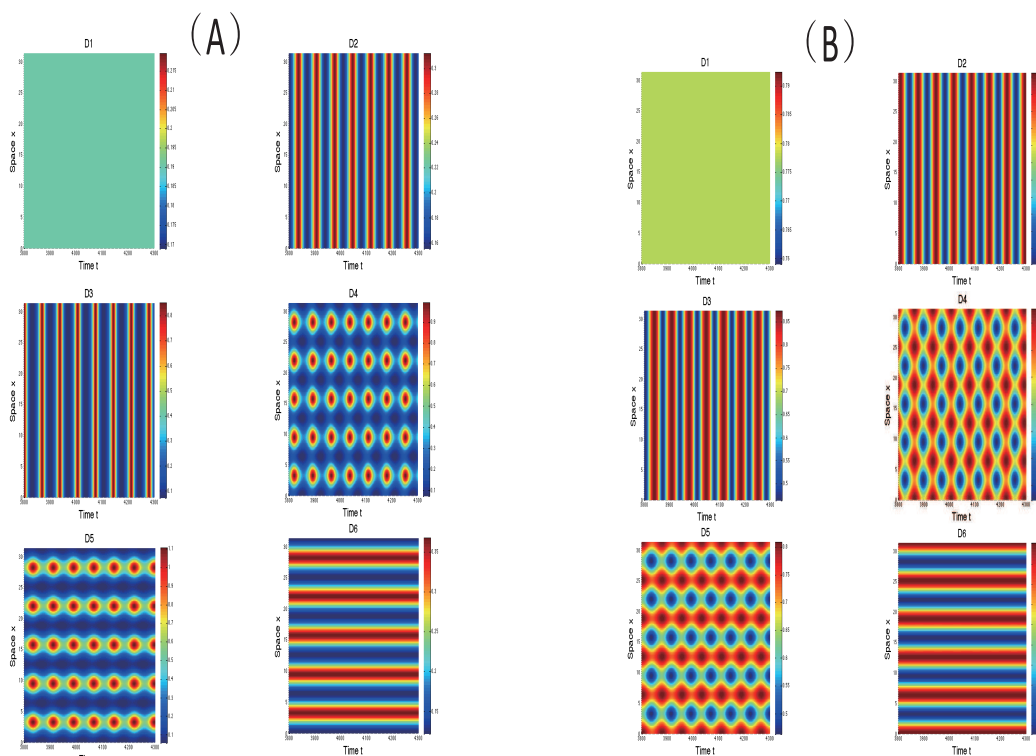


Figure 3. Spatiotemporal dynamics of model system (2.3) on mussel (A) and algae (B), where the color depicts the dimensionless values of the mussel density and algal concentration. The horizontal and vertical axis represent the space and time, respectively.

$$T_1^* : 0.1571\varepsilon_1 - 0.0646\varepsilon_2 = 0, \varepsilon_1 < 0;$$

$$T_2^* : 0.0260\varepsilon_1 + 0.1795\varepsilon_2 = 0, \varepsilon_1 > 0.$$

See Figure 7 for the comparison of the dynamics of (2.3) with or without terms  $\varepsilon_1^i \varepsilon_2^j \rho$  and  $\varepsilon_1^i \varepsilon_2^j s$ . In the  $\varepsilon_1 - \varepsilon_2$  plain, if we choose the point  $P(-0.01, -0.0038)$  without the terms  $\varepsilon_1^i \varepsilon_2^j \rho$  and  $\varepsilon_1^i \varepsilon_2^j s$  in the normal form, then  $P \in D_6$  shows that  $E^*$  is unstable. However, with these terms, we can obtain more accurate dynamical information since  $P \in D_1$ , not  $P \in D_6$ , so the positive spatially homogeneous steady state  $E^*$  is stable; see Figure 8.

**3.3.2. The dynamics away from the TH bifurcation point.** As we know, the method provided previously is efficient for the sufficiently small neighborhood of the TH bifurcation point. For the parameters away from such point, there may be more interactions of Turing and Hopf modes, and the corresponding dynamics are much more complicated, and the theoretical analysis is even more difficult. In the following, we numerically investigate the spatiotemporal dynamics for the parameters away from the TH bifurcation point.

For fixed  $\varepsilon_1 = 0.01$ , Figure 9 illustrates the final stable spatiotemporal patterns with decreasing of  $\varepsilon_2$ , which shows the shifting from spatially inhomogeneous periodic solutions to spatially inhomogeneous steady state when the mussel-algae diffusivity ratio  $\mu$  is decreasing.

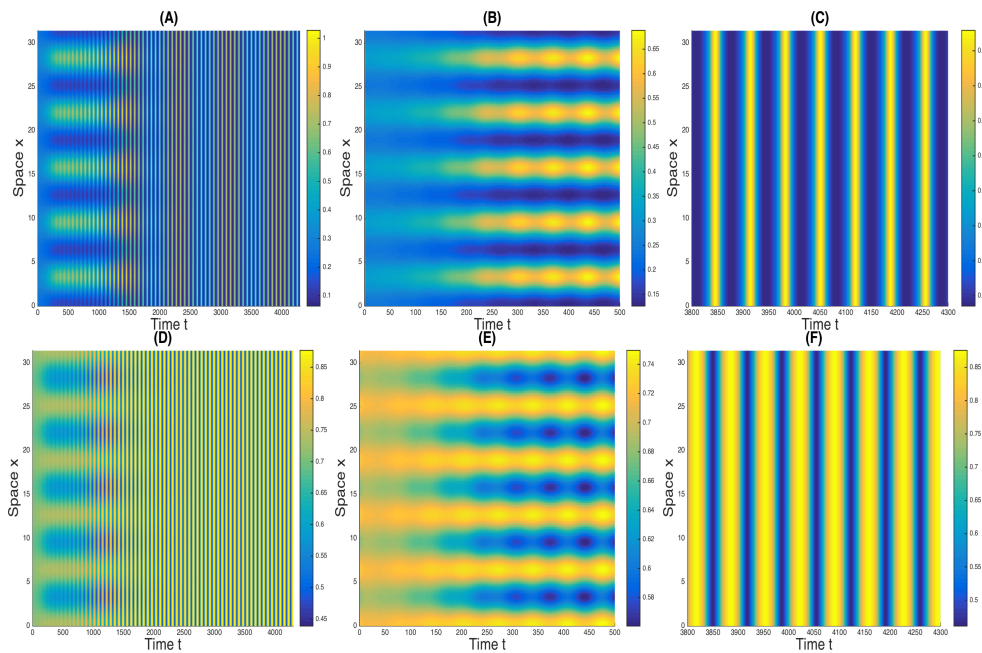


**Figure 4.** When  $(\varepsilon_1, \varepsilon_2) = (0.02, 0.001) \in D_3$  and the initial values are  $(m_0, a_0) = (0.2824 - 0.05 \cos x, 0.7025 + 0.03 \cos x)$ , the positive constant steady state  $E^*$  of system (2.3) is unstable. (A)–(C): The dynamics of mussel; (D)–(F): The dynamics of algae. There are unstable spatially inhomogeneous steady states and stable homogeneous periodic solutions, so there exists an orbit connecting these two states.

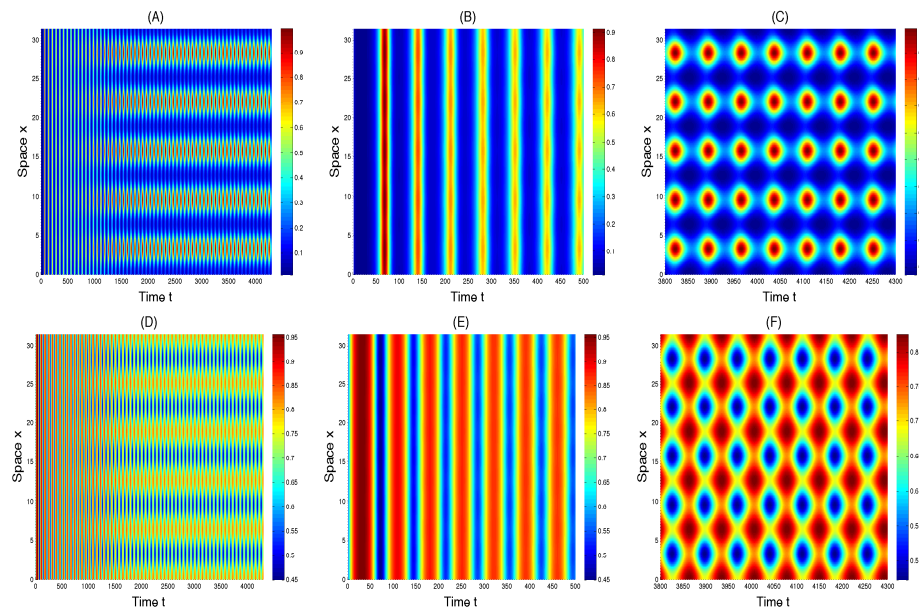


**Figure 5.** When  $(\varepsilon_1, \varepsilon_2) = (0.01, -0.003) \in D_4$  and the initial values are  $(m_0, a_0) = (0.15 - 0.005 \cos x, 0.5 - 0.005 \cos x)$ , the positive constant steady state  $E^*$  of system (2.3) is unstable. (A)–(C): The dynamics of mussel; (D)–(F): The dynamics of algae. There are unstable spatially homogeneous periodic solution and stable spatially inhomogeneous periodic solutions, so there exists an orbit connecting these two states.

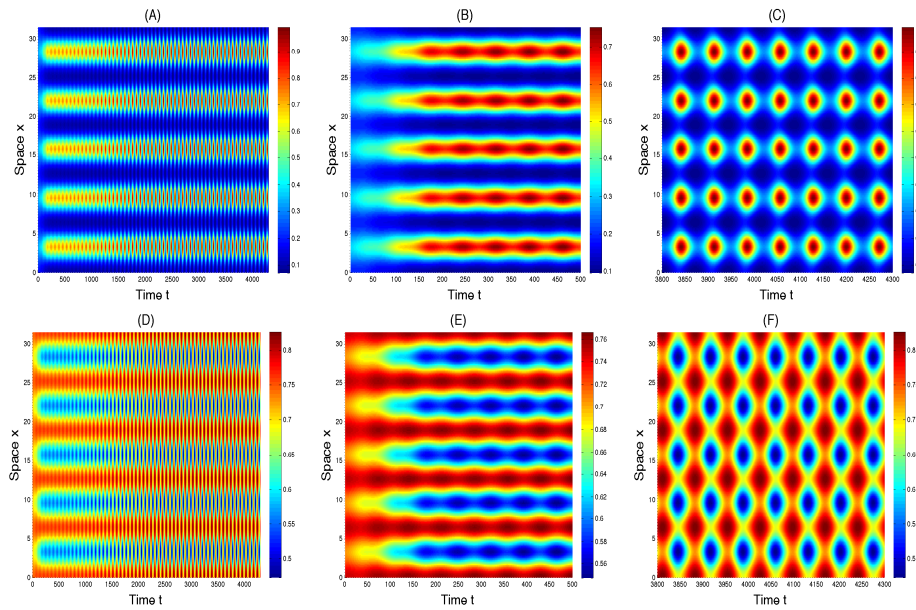


**Figure 6.** When  $(\varepsilon_1, \varepsilon_2) = (0.01, -0.003) \in D_4$  and the initial values are  $(m_0, a_0) = (0.2503 - 0.06 \cos x, 0.7270 + 0.02 \cos x)$ , the positive constant steady state  $E^*$  of system (2.3) is unstable. (A)–(C): The dynamics of mussel; (D)–(F): The dynamics of algae. There are unstable spatially inhomogeneous steady states and stable spatially inhomogeneous periodic solutions, so there exists an orbit connecting these two states.

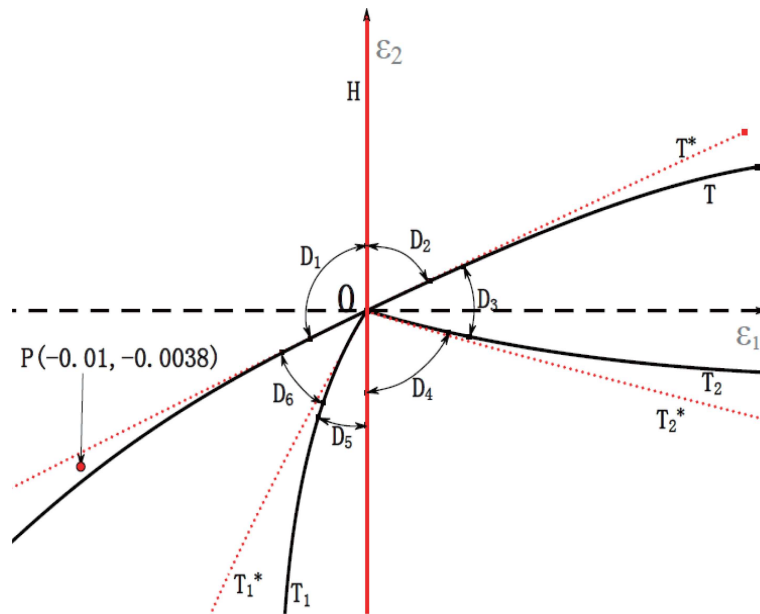


**Figure 7.** Comparison of bifurcation diagram of the normal form system (3.11) with (solid curves) or without (dashed lines) the terms  $\varepsilon_1^i \varepsilon_2^j \rho$  and  $\varepsilon_1^i \varepsilon_2^j s$  with  $i + j = 2$ .

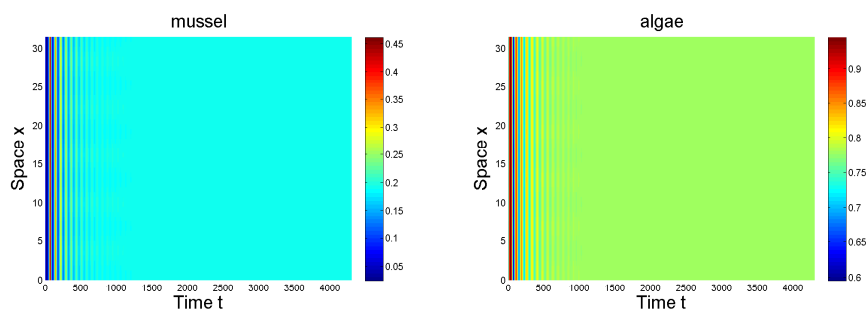


**Figure 8.** When  $(\varepsilon_1, \varepsilon_2) = (-0.01, -0.0038)$  and the initial values are  $(m_0, a_0) = (0.15 - 0.005 \cos x, 0.6 - 0.005 \cos x)$ , the positive constant steady state  $E^*$  of system (2.3) is asymptotically stable.

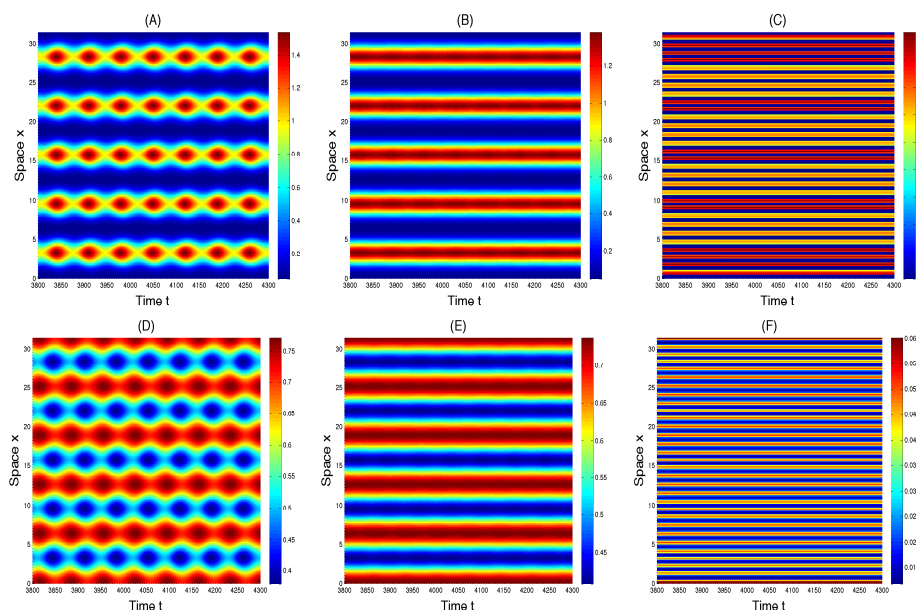


**Figure 9.** For fixed  $\varepsilon_1 = 0.01$ , the dynamics is changed with the decreasing of  $\varepsilon_2$ . (A) and (D):  $\varepsilon_2 = -0.013$  and spatially inhomogeneous periodic solutions; (B) and (E):  $\varepsilon_2 = -0.015$  and spatially inhomogeneous steady state with wide strips; (C) and (F):  $\varepsilon_2 = -0.052$  and spatially inhomogeneous steady state with narrow strips. (A)–(C): The dynamics of mussel; (D)–(F): The dynamics of algae.

Comparing with Figure 6(C,F), where  $\varepsilon_2 = -0.003$ , we can see that when  $\varepsilon_2 = -0.013$ , the spatially inhomogeneous periodic solution remains, and it disappears as  $\varepsilon_2 \leq -0.015$  with the occurrence of the spatially inhomogeneous steady state with strips.

**3.3.3. The influence of the advection on the dynamics.** To the best of our knowledge, in the literature there is no theoretical work done yet about the normal form computation in the model with the advection term, which is not trivial. Here we discuss the influence of advection on the system (2.2) by using the numerical method. Comparing with Figure 3, where there is no advection involved in the system, we can observe the motion change due to the introduction of the advection, such as the loss of the stability of the steady state and the break

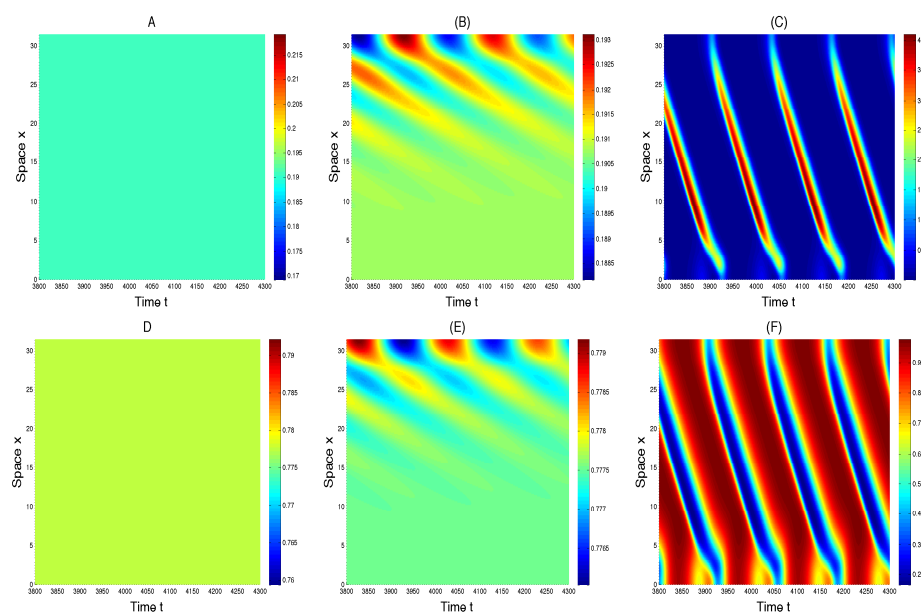


**Figure 10.** When  $(\varepsilon_1, \varepsilon_2) = (-0.01, 0.001) \in D_1$ , the dynamics is changed with the increasing of the value of advection  $\nu$ .  $\nu = 0.4$  for (A) and (D),  $\nu = 0.42$  for (B) and (E), and  $\nu = 0.8$  for (C) and (F). (A)–(C): The dynamics of mussel; (D)–(F): The dynamics of algae.

of the spatially homogeneous oscillations. For instance, when  $(\varepsilon_1, \varepsilon_2) = (-0.01, 0.001) \in D_1$ , the steady state of (2.3) is stable (see Figure 3(A(D1),B(D1))). Such stability stays for small advection and loses the stability when the advection value reaches a critical value (see Figure 10). When  $(\varepsilon_1, \varepsilon_2) = (0.02, 0.001) \in D_2$  or  $(\varepsilon_1, \varepsilon_2) = (0.01, -0.003) \in D_4$ , by the comparison of the figures, i.e., Figure 11 vs. Figure 3 (A(D2),B(D2)) and Figure 12 vs. Figure 3(A(D4),B(D4)), respectively, we can view the connecting dynamics showing the loss of stable spatially homogeneous steady state or oscillation.

**4. Discussion and conclusion.** In this paper, we have derived the normal form computation for a general reaction-diffusion equation by taking the effect of diffusion into account, then applying the results to study TH bifurcation for the diffusive mussel-algae model under the homogeneous Neumann boundary condition.

The stability and Hopf bifurcation of the positive equilibrium of the corresponding ODE system (2.4) is determined according to the parameters  $r$  (a measure of the growth rate of mussel) and  $\gamma$  (a parameter indicates the mortality of mussels). When  $\gamma$  is less than the critical value  $\gamma_{min}^*$ , the positive equilibrium is always stable independent of  $r$ . However, when  $\gamma$  is larger than  $\gamma_{min}^*$ ,  $r$  plays an important role in determining the stability of the positive equilibrium and the existence of Hopf bifurcation, and it can lead to periodic oscillation.

For the diffusive mussel-algae model, we discuss the mussel-algae diffusivity ratio  $\mu$  and the growth rate  $r$  of mussel on the stability and TH bifurcation of the positive steady state of systems (2.3). More precisely, if we fixed  $\gamma$  less than  $\gamma_{min}^*$ , there is no TH bifurcation, and only diffusion-driven Turing instability occurs. When  $\gamma$  is sufficiently small, the authors have investigated in detail the Turing patterns for two-dimensional spatial variables and found

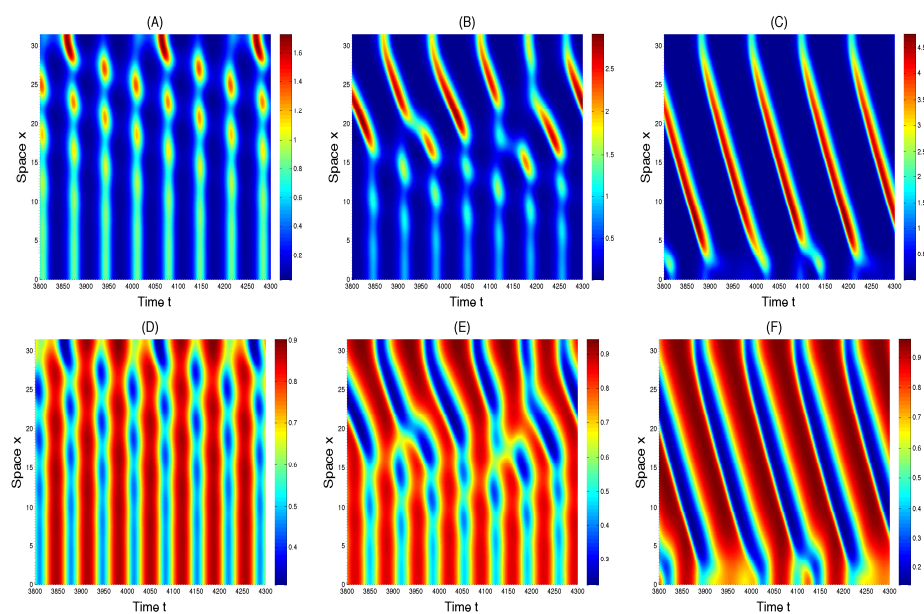


**Figure 11.** When  $(\varepsilon_1, \varepsilon_2) = (0.02, 0.001) \in D_2$ , the dynamics is changed with the increasing of the value of advection  $\nu$ .  $\nu = 0.38$  for (A) and (D),  $\nu = 0.46$  for (B) and (E), and  $\nu = 0.8$  for (C) and (F). (A)–(C): The dynamics of mussel; (D)–(F): The dynamics of algae.

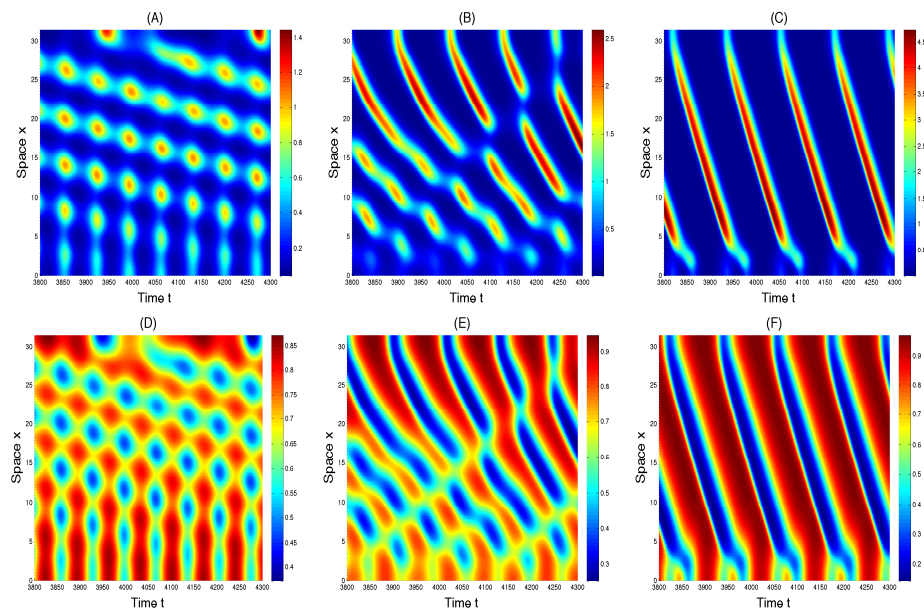


**Figure 12.** When  $(\varepsilon_1, \varepsilon_2) = (0.01, -0.003) \in D_4$ , the dynamics is changed with the increasing of the value of advection  $\nu$ .  $\nu = 0.2$  for (A) and (D),  $\nu = 0.4$  for (B) and (E), and  $\nu = 0.8$  for (C) and (F). (A)–(C): The dynamics of mussel; (D)–(F): The dynamics of algae.

different patterns, such as rhombic or hexagonal arrays and isolated clusters of clumps or gaps, an intermediate labyrinthine state by employing weakly nonlinear diffusive instability analyses in [3]. However, we show that the critical value  $\gamma_{min}^*$  is analytically determined.

If we fixed  $\gamma$  larger than  $\gamma_{min}^*$ , which is not considered in [3], the stability, Turing instability, and TH bifurcation of the positive steady state of system (2.3) is investigated according to the potential growth rate  $r$  of mussel and the mussel-algae diffusivity ratio  $\mu$ . When  $\mu$  is fixed and larger than the critical value, the system (2.3) first undergoes Hopf bifurcation and then Turing bifurcation as  $r$  is increasing, while when  $\mu$  is fixed and smaller than the critical value, the story is reverse; i.e., the system (2.3) first undergoes Turing bifurcation and then Hopf bifurcation. Furthermore, the spatiotemporal dynamical classification near the TH bifurcation point is investigated in detail by using normal form theory. The parameter regions for occurrence of stable spatial homogeneous/homogeneous periodic solutions and stable homogeneous/homogeneous steady states are explicitly determined. We also found three types of pattern transitions, which are also called oscillatory Turing patterns and previously found using numerical method in [62, 63]. Stable spatial homogeneous periodic solutions make up another new foundation, which is the result of interaction of Turing bifurcation and Hopf bifurcation and cannot occur for only Hopf bifurcation or Turing bifurcation.

From numerical simulations, it is easy to observe that the diffusion  $\mu$  and the growth rate  $r$  of mussel could result in complex dynamics of system (2.3). It is well known that the resulting spatial complexity is characteristic of many natural ecosystems. The mussel beds are spatial homogeneously distribution and spatial inhomogeneously distribution by varying the diffusion  $\mu$  of mussel, which imply that the diffusive instabilities might explain instances of spatial irregularities for natural communities. The growth rate  $r$  of mussel also reflects the interaction relationship between mussel and algae. So, the spatial distribution of algae is effected by the quantitative changes of mussel.

A very conspicuous features of patterned mussel beds is that they can develop from two different paths caused by the TH bifurcation (see Figures 5 and 6). These patterns display a coherent spatiotemporal oscillation behavior. Recently, it is reported in [20] that the pattern formation displays contrary ecosystem functioning arising from different ecological processes in spite of similar spatial patterns emergence. Hence, it is interesting to further explore the patterns stability and their ecological functions underlying the TH bifurcation in future work. One of the most relative functions is to clarify their differences of the ecological resilience following disturbance near the TH bifurcation. In the model of van de Koppel et al. [50] for pattern formation in mussel beds, a constant inshore advection of algae for the tidal flow is assumed. There are two aspects that should be extended and further improved in this model. First, in reality, the direction of advection oscillates with the tide. This periodic oscillation remarkably affects the development of spatial patterns on mussel beds [42]. Going beyond this advection, algal cells always disperse with Brownian motion in the water [8]. Particularly, this random Brownian movement behavior dominates the algae behavior in the boundary layer. Toward our objective to investigate the way in which these dispersion processes affect the potential for pattern formation, we have shown the four different spatial patterns underlying the assumption of dispersion processes, which were not identified in previous studies [3] of this models. Understanding the dynamics of mussel beds is an important topic due to its

economical benefit in many parts of the world. Predicting their spatiotemporal behaviors is an important step for restoration programs and mussel fisheries.

In ecosystems, one of the most intriguing functions of the spatial patterning is acting as the indicator for impending regime shift [31, 40] and ecological degradations [13]. Currently, such a significant ecological role is understood only by the pure Turing instability scenarios with linear stability predictions [6, 20]. There is a lack of a full comprehension of the spatial nonlinear dynamical behaviors, such as local patterns and hysteresis phenomena, in many ecosystems [39, 41, 42]. Our bifurcation analysis reveals that the indicator function may disappear when the relevant parameters lie in the TH bifurcation region, for example, in Figure 3(D2,D5), where the alternative emergencies of spatial patterns (or biomass) ascribe the time-series oscillations rather than the environmental degradation. Hence, analyzing the TH interactions could help us understand the ecosystems functioning—resilience and catastrophic shift—on spatial self-organization patterning.

In modeling the mussel bed ecosystems, the advection term is usually used to depict the tidal fluid direction where the water come from the sea to coast, and the diffusion term depicts the isotropic dispersion on horizontal planes. Although they are involved in two different ecological processes, advection and diffusion terms have the same mechanism—an active-inhibitor principle [21]. For the emergent properties of spatial self-organization patterns, the advection and diffusion are equivalent. With both advection and diffusion in the algal equation based on the van de Koppel model, one could use a dimensionless pecelet number—a ratio related to these two processes to describe the influence of the joint effects that is beyond the scope of this paper. It is shown in [42, 52] that the qualitative properties are similar, although there is a slight difference in the quantitative prediction of onset of spatial patterns. How do we predict the dynamical behavior theoretically for the system with both advection and diffusion terms explicitly? We leave this as a potential topic for future research.

#### Appendix A. Calculation of the $B_{1j}, B_{2j}, B_{3j}, j = 1, 2$ .

$$B_{11} = C_{11} + \frac{3}{2} (D_{11} + E_{11}) = \overline{B_{21}}, \quad B_{31} = C_{31} + \frac{3}{2} (D_{31} + E_{31}),$$

$$B_{12} = C_{12} + \frac{3}{2} (D_{12} + E_{12}) = \overline{B_{2j}}, \quad B_{32} = C_{32} + \frac{3}{2} (D_{32} + E_{32}),$$

where

$$C_{11} = \frac{1}{2l\pi} q_0^T A_{210} = \overline{C_{21}}, \quad C_{12} = \frac{1}{2l\pi} q_0^T A_{102} = \overline{C_{22}}, \quad C_{31} = \frac{1}{l\pi} q_{k_*}^T A_{111}, \quad C_{32} = \frac{1}{4l\pi} q_{k_*}^T A_{003},$$

and

$$D_{11} = \frac{1}{3li\pi\omega_0} \left[ - (q_0^T A_{200}) (q_0^T A_{110}) + \frac{1}{3} (q_0^T A_{020}) (q_0^T A_{200}) + 2 (q_0^T A_{110})^2 \right] = \overline{D_{21}},$$

$$D_{12} = \frac{1}{3li\pi\omega_0} \left[ - (q_0^T A_{200}) (q_0^T A_{002}) + (q_0^T A_{110}) (\overline{q_0^T A_{002}}) + 2 (q_0^T A_{002}) (q_0^T A_{101}) \right] = \overline{D_{22}},$$

$$D_{31} = -\frac{1}{3l\pi\omega_0} \text{Im} \{ (q_0^T A_{110}) (q_{k_*}^T A_{101}) \}, \quad D_{32} = -\frac{2}{3l\pi\omega_0} \text{Im} \{ (q_0^T A_{002}) (q_{k_*}^T A_{101}) \},$$

and

$$\begin{aligned}
 E_{11} &= \frac{1}{3\sqrt{l\pi}} q_0^T [H_2(0, p_0, h_{0110}) + H_2(\overline{0}, \overline{p_0}, h_{0200})] = \overline{E_{21}}, \\
 E_{12} &= \frac{1}{3\sqrt{l\pi}} q_0^T [H_2(0, p_0, h_{0002}) + H_2(0, p_{k^*}, h_{k^*101})] = \overline{E_{22}}, \\
 E_{31} &= \frac{1}{3\sqrt{l\pi}} q_{k^*}^T [H_2(0, p_0, h_{k^*011}) + H_2(0, \overline{p_0}, h_{k^*101}) \\
 &\quad + H_2(0, p_{k^*}, h_{0110})] + \frac{1}{3\sqrt{2l\pi}} q_{k^*}^T H_2(0, p_{k^*}, h_{(2k^*)110}), \\
 E_{32} &= \frac{1}{3\sqrt{l\pi}} q_{k^*}^T H_2(0, p_{k^*}, h_{0002}) + \frac{1}{3\sqrt{2l\pi}} q_{k^*}^T H_2(0, p_{k^*}, h_{(2k^*)002}),
 \end{aligned}$$

with

$$\begin{aligned}
 h_{0200} &= \frac{1}{\sqrt{l\pi}} (2i\omega_0 I - \mathcal{M}_0)^{-1} (A_{200} - q_0^T A_{200} p_0 - \overline{q_0}^T A_{200} \overline{p_0}), \\
 h_{0020} &= \frac{1}{\sqrt{l\pi}} (-2i\omega_0 I - \mathcal{M}_0)^{-1} (A_{020} - q_0^T A_{020} p_0 - \overline{q_0}^T A_{020} \overline{p_0}), \\
 h_{0002} &= -\frac{1}{\sqrt{l\pi}} \mathcal{M}_0^{-1} (A_{002} - q_0^T A_{002} p_0 - \overline{q_0}^T A_{002} \overline{p_0}), \\
 h_{0110} &= -\frac{2}{\sqrt{l\pi}} \mathcal{M}_0^{-1} (A_{110} - q_0^T A_{110} p_0 - \overline{q_0}^T A_{110} \overline{p_0}), \\
 h_{k^*101} &= \frac{2}{\sqrt{l\pi}} (i\omega_0 I - \mathcal{M}_{k^*})^{-1} (A_{101} - q_{k^*}^T A_{101} p_{k^*}), \\
 h_{k^*011} &= \frac{2}{\sqrt{l\pi}} (-i\omega_0 I - \mathcal{M}_{k^*})^{-1} (A_{011} - q_{k^*}^T A_{011} p_{k^*}), \\
 h_{(2k^*)002} &= -\frac{1}{\sqrt{2l\pi}} \mathcal{M}_{2k^*}^{-1} A_{002}, \quad h_{(2k^*)110} = (0, 0)^T.
 \end{aligned}$$

**Appendix B. Calculation of  $B_i^{(1)}, B_i^{(2)}, i = 1, 2, 3$ , and  $B_{1j}, B_{2j}, B_{3j}, j = 3, 4, 5$ .**

By the previous results of [46, 47] and (3.4), we obtain  $f_2^1(z, 0, \varepsilon)$  as follows:

(B.1)

$$f_2^1(z, 0, \varepsilon) = \Psi(0) \left( \begin{array}{c} \left[ 2 \left( \left( \begin{array}{c} \varepsilon^2 \frac{\partial^2}{\partial x^2} \\ 0 \end{array} \right) + L_1(\varepsilon_1) \right) (\Phi z_x) + F_2(\Phi z_x, \varepsilon_1), \beta_\nu^{(1)} \right]_{\nu=k^*} \\ \left[ 2 \left( \left( \begin{array}{c} \varepsilon^2 \frac{\partial^2}{\partial x^2} \\ 0 \end{array} \right) + L_1(\varepsilon_1) \right) (\Phi z_x) + F_2(\Phi z_x, \varepsilon_1), \beta_\nu^{(2)} \right]_{\nu=0} \end{array} \right),$$

where  $\Psi(0) = \text{diag}\{\Psi_0, \Psi_{k^*}\}$ , and

$$\begin{aligned}
 &\left( \left( \left( \begin{array}{c} \varepsilon^2 \frac{\partial^2}{\partial x^2} \\ 0 \end{array} \right) + L_1(\varepsilon_1) \right) (\Phi z_x) \right. \\
 &\quad = P_{10010} z_1 \varepsilon_1 \gamma_0(x) + P_{01010} z_2 \varepsilon_1 \gamma_0(x) + P_{00110} z_3 \varepsilon_1 \gamma_{k^*}(x) + P_{00101} z_3 \varepsilon_2 \gamma_{k^*}(x),
 \end{aligned}$$

where  $P_{10010}, P_{01010}, P_{00110}, P_{00101}$  are the coefficient of the second-order items  $z_1\varepsilon_1, z_2\varepsilon_1, z_3\varepsilon_1, z_3\varepsilon_2$ , respectively.

Since  $F(0, \varepsilon_1) = 0$  and  $DF(0, \varepsilon_1) = 0$ ,  $F(\Phi z_x + w, \varepsilon_1)$  can be written as follows:

$$\begin{aligned} F(\Phi z_x + w, \varepsilon_1) &= F(\Phi z_x + w, 0) \\ &= \sum_{q_1+q_2+q_3=2} A_{q_1q_2q_3} \gamma_0^{q_1+q_2}(x) \gamma_{k_*}^{q_3}(x) z_1^{q_1} z_2^{q_2} z_3^{q_3} + H_2(\Phi z_x, w) + O(|w|^2), \end{aligned}$$

where  $H_2$  includes the product terms of  $\Phi z_x$  and  $w$ ,  $q_1, q_2, q_3 \in \mathbb{N}_0$ ,  $A_{q_1q_2q_3} = (A_{q_1q_2q_3}^{(1)}, A_{q_1q_2q_3}^{(2)})$ , and  $A_{q_1q_2q_3}^{(j)} = \overline{A_{q_2q_1q_3}^{(j)}}$ ,  $j = 1, 2$ . Then, from (3.3) and (B.1), we have

(B.2)

$$\begin{aligned} f_2^1(z, 0, \varepsilon) &= \frac{1}{\sqrt{l\pi}} \Psi(0) \begin{pmatrix} A_{200} z_1^2 + A_{020} z_2^2 + A_{002} z_3^2 + 2A_{110} z_1 z_2 + 2\sqrt{l\pi} P_{10010} z_1 \varepsilon_1 + 2\sqrt{l\pi} P_{01010} z_2 \varepsilon_1 \\ 2A_{101} z_1 z_3 + 2A_{011} z_2 z_3 + 2\sqrt{l\pi} P_{00110} z_3 \varepsilon_1 + 2\sqrt{l\pi} P_{00101} z_3 \varepsilon_2 \end{pmatrix}. \end{aligned}$$

Therefore, by (3.6) and (B.2), we get

(B.3)

$$g_2^1(z, 0, \varepsilon) = Proj_{Ker(M_2^1)} f_2^1(z, 0, \varepsilon) = \begin{pmatrix} (B_1^{(1)} \varepsilon_1 + B_1^{(2)} \varepsilon_2) z_1 + B_1^{(3)} z_1 z_3 \\ (B_2^{(1)} \varepsilon_1 + B_2^{(2)} \varepsilon_2) z_2 + B_2^{(3)} z_2 z_3 \\ (B_3^{(1)} \varepsilon_1 + B_3^{(2)} \varepsilon_2) z_3 + B_3^{(3)} z_1 z_2 + B_3^{(4)} z_3^2 \end{pmatrix},$$

where

$$\begin{aligned} B_1^{(1)} &= q_0^T P_{10010} = \overline{B_2^{(1)}}, \quad B_1^{(2)} = \overline{B_2^{(2)}} = 0, \quad B_1^{(3)} = \overline{B_2^{(3)}} = 0, \\ B_3^{(1)} &= q_{k_*}^T P_{00110}, \quad B_3^{(2)} = q_{k_*}^T P_{00101}, \quad B_3^{(3)} = 0, \quad B_3^{(4)} = 0. \end{aligned}$$

Following the results of [46, 47] and (3.7), we have  $g_3^1(z, 0, \varepsilon)$  as follows:

$$g_3^1(z, 0, \varepsilon) = Proj_{Ker(M_3^1)} \tilde{f}_3^1(z, 0, \varepsilon) = Proj_{S_1 \cup S_2} \tilde{f}_3^1(z, 0, \varepsilon) + O(|z|^2|\varepsilon|),$$

where

$$S_1 = span \{ z_1^2 z_2 e_1, z_1 z_3^2 e_1, z_1 z_2^2 e_2, z_2 z_3^2 e_2, z_1 z_2 z_3 e_3, z_3^3 e_3 \},$$

and

$$S_2 = span \{ z_1 \varepsilon_1^2 e_1, z_1 \varepsilon_2^2 e_1, z_1 \varepsilon_1 \varepsilon_2 e_1, z_2 \varepsilon_1^2 e_2, z_2 \varepsilon_2^2 e_2, z_2 \varepsilon_1 \varepsilon_2 e_2, z_3 \varepsilon_1^2 e_3, z_3 \varepsilon_2^2 e_3, z_3 \varepsilon_1 \varepsilon_2 e_3 \},$$

and  $\frac{1}{3!} \tilde{f}_3^1$  is term of order 3 obtained after the changes of variables in the previous step given by

$$\begin{aligned} \tilde{f}_3^1(z, 0, \varepsilon) &= f_3^1(z, 0, \varepsilon) + \frac{3}{2} [(D_z f_2^1)(z, 0, \varepsilon) U_2^1(z, \varepsilon) \\ &\quad + (D_w f_2^1)(z, 0, \varepsilon) U_2^2(z, \varepsilon) - (D_z U_2^1(z, \varepsilon)) g_2^1(z, 0, \varepsilon)], \end{aligned}$$

with

$$U_2^1(z, 0) = (M_2^1)^{-1} Proj_{Im(M_2^1)} f_2^1(z, 0, \varepsilon)$$

and

$$(M_2^1 U_2^2)(z, \varepsilon) = f_2^2(z, 0, \varepsilon).$$

Song et al. [46, 47] have computed the third-order term normal form in the subspace  $S_1$ ; we provide mainly the third-order term normal form in the subspace  $S_2$ . Hence, we need to calculate the  $B_{1j}, B_{2j}, B_{3j}, j = 3, 4, 5$  step by step.

*Step 1.* The calculation of  $C_{1j}, C_{2j}, C_{3j}, j = 3, 4, 5$ .

From [46, 47] and (3.4), we obtain  $f_3^1(z, 0, \varepsilon)$  as follows:

$$(B.4) \quad f_3^1(z, 0, \varepsilon) = \Psi(0) \left( \begin{array}{c} \left[ 3L_2(\varepsilon_1)(\Phi z_x) + F_3(\Phi z_x, \varepsilon_1), \beta_\nu^{(1)} \right] \\ \left[ 3L_2(\varepsilon_1)(\Phi z_x) + F_3(\Phi z_x, \varepsilon_1), \beta_\nu^{(2)} \right] \end{array} \right)_{\nu=0}^{\nu=k_*},$$

where  $L_2(\varepsilon_1) = P_{10020} z_1 \varepsilon_1^2 + P_{01020} z_2 \varepsilon_1^2 + P_{00120} z_3 \varepsilon_1^2$  and

$$F_3(\Phi z_x, 0) = \sum_{q_1+q_2+q_3=3} A_{q_1 q_2 q_3} \gamma_0^{q_1+q_2}(x) \gamma_{k_*}^{q_3}(x) z_1^{q_1} z_2^{q_2} z_3^{q_3}, \quad A_{q_1 q_2 q_3} = \overline{A_{q_2 q_1 q_3}}.$$

Then, from (3.3) and (B.4), we have

$$(B.5) \quad f_3^1(z, 0, \varepsilon) = \frac{1}{l\pi} \Psi(0) \left( \begin{array}{c} A_{300} z_1^3 + A_{210} z_1^2 z_2 + A_{102} z_1 z_2^2 + A_{012} z_2 z_3^2 + l\pi P_{10020} z_1 \varepsilon_1^2 + l\pi P_{01020} z_1 \varepsilon_1^2 \\ A_{201} z_1^2 z_3 + A_{021} z_2^2 z_3 + A_{111} z_1 z_2 z_3 + A_{003} z_3^3 + l\pi P_{00120} z_3 \varepsilon_1^2 \end{array} \right).$$

Therefore, by (B.5), we get

$$(B.6) \quad \frac{1}{3!} Proj_{S_2} f_3^1(z, 0, \varepsilon) = \left( \begin{array}{c} C_{13} z_1 \varepsilon_1^2 + C_{14} z_1 \varepsilon_2^2 + C_{15} z_1 \varepsilon_1 \varepsilon_2 \\ C_{23} z_2 \varepsilon_1^2 + C_{24} z_2 \varepsilon_2^2 + C_{25} z_2 \varepsilon_1 \varepsilon_2 \\ C_{33} z_3 \varepsilon_1^2 + C_{34} z_3 \varepsilon_2^2 + C_{35} z_3 \varepsilon_1 \varepsilon_2 \end{array} \right),$$

where

$$C_{13} = \frac{1}{2} q_0^T P_{10020} = \overline{C_{23}}, \quad C_{14} = \overline{C_{24}} = 0, \quad C_{15} = \overline{C_{25}} = 0, \quad C_{33} = \frac{1}{2} q_{k_*}^T P_{00120}, \quad C_{34} = C_{35} = 0.$$

*Step 2.* The calculation of  $D_{1j}, D_{2j}, D_{3j}, j = 3, 4, 5$ .

From (B.2), we have

$$(B.7) \quad U_2^1(z, \varepsilon) = (M_2^1)^{-1} Proj_{(Im M_2^1)} f_2^1(z, 0, \varepsilon) = \frac{1}{i\omega_0 \sqrt{l\pi}} \left( \begin{array}{c} q_0^T \left( A_{200} z_1^2 - \frac{1}{3} A_{020} z_2^2 - A_{002} z_3^2 - 2A_{110} z_1 z_2 - \sqrt{l\pi} P_{01010} z_2 \varepsilon_1 \right) \\ \bar{q}_0^T \left( \frac{1}{3} A_{200} z_1^2 - A_{020} z_2^2 + A_{002} z_3^2 + 2A_{110} z_1 z_2 + \sqrt{l\pi} P_{10010} z_1 \varepsilon_1 \right) \\ q_{k_*}^T (2A_{101} z_1 z_3 - 2A_{011} z_2 z_3) \end{array} \right).$$

Then, by (B.2) and (B.7), we get

$$(B.8) \quad \frac{1}{3!} \text{Proj}_{S_2} (D_z f_2^1) (z, 0, \varepsilon) U_2^1(z, \varepsilon) = \begin{pmatrix} D_{13} z_1 \varepsilon_1^2 + D_{14} z_1 \varepsilon_2^2 + D_{15} z_1 \varepsilon_1 \varepsilon_2 \\ D_{23} z_2 \varepsilon_1^2 + D_{24} z_2 \varepsilon_2^2 + D_{25} z_2 \varepsilon_1 \varepsilon_2 \\ D_{33} z_3 \varepsilon_1^2 + D_{34} z_3 \varepsilon_2^2 + D_{35} z_3 \varepsilon_1 \varepsilon_2 \end{pmatrix},$$

where

$$D_{13} = \frac{1}{3li\omega_0} [- (q_0^T P_{01010}) (\bar{q}_0^T P_{10010})] = \overline{D_{23}},$$

$$D_{14} = \overline{D_{24}} = 0, \quad D_{15} = \overline{D_{25}} = 0, \quad D_{33} = D_{34} = D_{35} = 0.$$

*Step 3.* The calculation of  $E_{1j}, E_{2j}, E_{3j}$ ,  $j = 3, 4, 5$ .

Let

$$U_2^2(z, \varepsilon) \doteq h(z, \varepsilon) = \sum_{k \geq 0} h_k(z, \varepsilon) \beta_k$$

with

$$(B.9) \quad h_k(z, \varepsilon) = \begin{pmatrix} h_k^{(1)}(z, \varepsilon) \\ h_k^{(2)}(z, \varepsilon) \end{pmatrix} = \sum_{q_1+q_2+q_3=2} \begin{pmatrix} h_{kq_1q_2q_3}^{(1)} \\ h_{kq_1q_2q_3}^{(2)} \end{pmatrix} z_1^{q_1} z_2^{q_2} z_3^{q_3} + \sum_{s=1}^3 \left( \begin{pmatrix} h_{ks1}^{(1)} \\ h_{ks1}^{(2)} \end{pmatrix} z_s \varepsilon_1 + \begin{pmatrix} h_{ks2}^{(1)} \\ h_{ks2}^{(2)} \end{pmatrix} z_s \varepsilon_2 \right).$$

Then, by (3.7), (B.2), and (B.9), we obtain

$$(B.10) \quad \frac{1}{3!} \text{Proj}_{S_2} (D_w f_2^1) (z, 0, \varepsilon) U_2^2(z, \varepsilon) = \begin{pmatrix} E_{13} z_1 \varepsilon_1^2 + E_{14} z_1 \varepsilon_2^2 + E_{15} z_1 \varepsilon_1 \varepsilon_2 \\ E_{23} z_2 \varepsilon_1^2 + E_{24} z_2 \varepsilon_2^2 + E_{25} z_2 \varepsilon_1 \varepsilon_2 \\ E_{33} z_3 \varepsilon_1^2 + E_{34} z_3 \varepsilon_2^2 + E_{35} z_3 \varepsilon_1 \varepsilon_2 \end{pmatrix},$$

where

$$E_{13} = \frac{1}{3} q_0^T H_2 (\varepsilon_1, 0, h_{011}) = \overline{E_{23}}, \quad E_{14} = \overline{E_{24}} = 0, \quad E_{15} = \overline{E_{25}} = 0,$$

$$E_{33} = \frac{1}{3} q_{k_*}^T H_2 (\varepsilon_1, 0, h_{k_*31}), \quad E_{34} = \frac{1}{3} q_{k_*}^T H_2 (\varepsilon_2, 0, h_{k_*32}),$$

$$E_{35} = \frac{1}{3} q_{k_*}^T (H_2 (\varepsilon_2, 0, h_{k_*31}) + H_2 (\varepsilon_1, 0, h_{k_*32})),$$

with the computation of  $h_{011}(z, \varepsilon), h_{021}(z, \varepsilon), h_{k_*31}(z, \varepsilon), h_{k_*32}(z, \varepsilon)$ ; see Appendix C.

**Appendix C. Computation of  $h_{011}(z, \varepsilon), h_{021}(z, \varepsilon), h_{k_*31}(z, \varepsilon), h_{k_*32}(z, \varepsilon)$ , respectively.** (1). Computation of  $h_{011}(z, \varepsilon)$  and  $h_{021}(z, \varepsilon)$  from

$$(i\omega_0 I - \mathcal{M}_0) h_{011} = 2 (P_{10010} - q_0^T P_{10010} p_0 - \bar{q}_0^T P_{10010} \bar{p}_0),$$

$$(i\omega_0 I - \mathcal{M}_0) h_{021} = 2 (P_{01010} - q_0^T P_{01010} p_0 - \bar{q}_0^T P_{01010} \bar{p}_0).$$

Since  $i\omega_0$  is an eigenvalue of  $\mathcal{M}_0$ , the matrix  $i\omega_0 I - \mathcal{M}_0$  is not invertible, and the linear system  $Dw = a$  may not have solutions. According to [15],  $h_{0j1}$  can be determined by solving the following bordered system:

$$\begin{pmatrix} (i\omega_0 I - \mathcal{M}_0) & p_0 \\ q_0^T & 0 \end{pmatrix} \begin{pmatrix} h_{0j1} \\ h \end{pmatrix} = \begin{pmatrix} E_j \\ 0 \end{pmatrix}, \quad j = 1, 2,$$

where  $h \in \mathbb{R}$  is an additional variable,

$$E_1 = 2(P_{10010} - q_0^T P_{10010} p_0 - \bar{q}_0^T P_{10010} \bar{p}_0), \quad E_2 = 2(P_{01010} - q_0^T P_{01010} p_0 - \bar{q}_0^T P_{01010} \bar{p}_0).$$

(2). Computation of  $h_{k_*31}(z, \varepsilon)$  and  $h_{k_*32}(z, \varepsilon)$  from

$$\begin{aligned} \mathcal{M}_{k_*} h_{k_*31} &= 2(P_{00110} - q_{k_*}^T P_{00110} p_{k_*}), \\ \mathcal{M}_{k_*} h_{k_*32} &= 2(P_{00101} - q_{k_*}^T P_{00101} p_{k_*}). \end{aligned}$$

Since 0 is an eigenvalue of  $\mathcal{M}_{k_*}$ , the matrix  $\mathcal{M}_{k_*}$  is not invertible, and the linear system  $Dw = a$  may not have solutions. According to [15],  $h_{k_*3j}$  can be overcome by solving the following bordered system:

$$\begin{pmatrix} \mathcal{M}_{k_*} & p_{k_*} \\ q_{k_*}^T & 0 \end{pmatrix} \begin{pmatrix} h_{k_*3j} \\ h \end{pmatrix} = \begin{pmatrix} F_j \\ 0 \end{pmatrix}, \quad j = 1, 2,$$

where  $h \in \mathbb{R}$  is an additional variable,

$$F_1 = 2(P_{00110} - q_{k_*}^T P_{00110} p_{k_*}), \quad F_2 = 2(P_{00101} - q_{k_*}^T P_{00101} p_{k_*}).$$

**Acknowledgments.** We would like to thank the editor and reviewers for their valuable comments and suggestions, which significantly improved the quality of our paper indeed.

## REFERENCES

- [1] F. BORGOGNO, P. D'ODORICO, F. LAIO, AND L. RIDOLFI, *Mathematical models of vegetation pattern formation in ecohydrology*, Rev. Geophys., 47 (2009), <https://doi.org/10.1029/2007RG000256>.
- [2] M. BAURMANN, T. GROSS, AND U. FEUDEL, *Instabilities in spatially extended predator-prey systems: spatio-temporal patterns in the neighborhood of Turing-Hopf bifurcations*, J. Theoret. Biol., 245 (2007), pp. 220–229.
- [3] R. A. CANGELOSI, D. J. WOLLKIND, B. J. KEALY-DICHONE, AND I. CHAIYA, *Nonlinear stability analyses of Turing patterns for a mussel-algae model*, J. Math. Biol., 70 (2015), pp. 1249–1294.
- [4] S. S. CHEN AND J. P. SHI, *Global attractivity of equilibrium in Gierer-Meinhardt system with activator production saturation and gene expression time delays*, Nonlinear Anal. RWA, 14 (2013), pp. 1871–1886.
- [5] M. C. CROSS AND P. C. HOHENBERG, *Pattern formation outside of equilibrium*, Rev. Mod. Phys., 65 (1993), pp. 835–844.
- [6] V. DAKOS, S. KÉFI, M. RIETKERK, E. H. VAN NES, AND M. SCHEFFER, *Slowing down in spatially patterned ecosystems at the brink of collapse vasilis*, Amer. Naturalist, 177 (6) (2011), pp. E153–E166.
- [7] J. J. A. DONKER, M. VAN DER VEGT, AND P. HOEKSTRA, *Erosion of an intertidal mussel bed by ice-and wave-action*, Continental Shelf Res., 106 (2015), pp. 60–69.

- [8] W. M. DURHAM, E. CLIMENT, M. BARRY, F. DE LILLO, G. BOFFETTA, M. CENCINI, AND R. STOCKER, *Turbulence drives microscale patches of motile phytoplankton*, Nat. Comm., 4 (2013), 2148.
- [9] T. FARIA, *Normal forms and Hopf bifurcation for partial differential equations with delay*, Trans. Amer. Math. Soc., 352 (2000), pp. 2217–2238.
- [10] T. FARIA, *Stability and bifurcation for a delayed predator-prey model and the effect of diffusion*, J. Math. Anal. Appl., 254 (2001), pp. 433–463.
- [11] G. H. GUO, B. F. LI, AND X. L. LIN, *Hopf bifurcation in spatially homogeneous and inhomogeneous autocatalysis models*, Comput. Math. Appl., 67 (2014), pp. 151–163.
- [12] A. GHAZARYAN AND V. MANUKIAN, *Coherent structures in a population model for mussel-algae interaction*, SIAM J. Appl. Dyn. Syst., 14 (2015), pp. 893–913.
- [13] S. KÉFI, M. RIETKERK., C. L. ALADOS, Y. PUEYO, V. P. PAPANASTASIS, A. ELAICH, AND P. C. DE RUITER, *Spatial vegetation patterns and imminent desertification in Mediterranean arid ecosystems*, Nature, 449 (2007), pp. 213–217.
- [14] C. A. KLAUSMEIER, *Regular and irregular patterns in semiarid vegetation*, Science, 285 (1999), pp. 838–838.
- [15] Y. A. KUZNETSOV, *Elements of Applied Bifurcation Theory*, 2nd ed., Springer-Verlag, New York, 1998.
- [16] X. LI AND W. H. JIANG, *Hopf bifurcation and Turing instability in the reaction-diffusion Holling-Tanner predator-prey model*, IMA J. Appl. Math., 78 (2013), pp. 287–306.
- [17] Q.-X. LIU, A. DOELMAN, V. ROTTSCHÄFER, M. D. JAGER, P. M. J. HERMAN, M. RIETKERK, AND J. VAN DE KOPPEL, *Phase separation explains a new class of self-organized spatial patterns in ecological systems*, Proc. Natl. Acad. Sci., 110 (2013), pp. 11905–11910.
- [18] Q.-X. LIU, P. M. J. HERMAN, W. M. MOOIJ, J. HUISMAN, M. SCHEFFER, H. OLFF, AND J. VAN DE KOPPEL, *Pattern formation at multiple spatial scales drives the resilience of mussel bed ecosystems*, Nat. Comm., 5 (2014), <https://doi.org/10.1038/ncomms6234>.
- [19] Q.-X. LIU, E. J. WEERMAN, R. GUPTA, P. M. J. HERMAN, H. OLFF, AND J. VAN DE KOPPEL, *Biogenic gradients in algal density affect the emergent properties of spatially self-organized mussel beds*, J. R. Soc. Interface, 6 (2014), pp. 2014–0089.
- [20] Q.-X. LIU, E. J. WEERMAN, P. M. J. HERMAN, H. OLFF, AND J. VAN DE KOPPEL, *Alternative mechanisms alter the emergent properties of self-organization in mussel beds*, Proc. R. Soc. B, 279 (2012), pp. 2744–2753.
- [21] Q.-X. LIU, M. RIETKERK, P. M. HERMAN, T. PIERSMA, J. M. FRYXELL, AND J. VAN DE KOPPEL, *Phase separation driven by density-dependent movement: a novel mechanism for ecological patterns*, Phys. Life Rev., (19) 2016, pp. 107–121.
- [22] M. J. MA AND J. J. HU, *Bifurcation and stability analysis of steady states to a Brusselator model*, Appl. Math. Comput., 236 (2014), pp. 580–592.
- [23] H. MEINHARDT, *Models of biological pattern formation*. Academic Press, London, 1982.
- [24] M. MEIXNER, A. DE WIT, S. BOSE, AND E. SCHOLL, *Generic spatiotemporal dynamics near codimension-two Turing-Hopf bifurcations*, Phys. Rev. E, 55 (1997), pp. 6690–6697.
- [25] H. MEINHARDT, P. PRUSINKIEWICZ, AND D. R. FOWLER, *The algorithmic beauty of sea shells*, 3rd ed., Springer, Berlin, 2003.
- [26] J. D. MURRAY, *Mathematical Biology II*, Springer-Verlag, Heidelberg, 2002.
- [27] Q. OUYANG AND H. L. SWINNEY, *Transition from a uniform state to hexagonal and striped Turing patterns*, Nature, 352 (1991), pp. 610–612.
- [28] R. PENG, *Asymptotic profiles of the positive steady state for an SIS epidemic reaction-diffusion model, part I*, J. Differential Equations, 247 (2009), pp. 1096–1119.
- [29] R. PENG AND F. Q. YI, *Asymptotic profile of the positive steady state for an SIS epidemic reaction-diffusion model: Effects of epidemic risk and population movement*, Phy. D, 259 (2013), pp. 8–25.
- [30] R. PENG, F. Q. YI, AND X. Q. ZHAO, *Spatiotemporal patterns in a reaction-diffusion model with the Degn-Harrison reaction scheme*, J. Differential Equations, 254 (2013), pp. 2465–2498.
- [31] M. RIETKERK, S. C. DEKKER, P. C. DE RUITER, AND J. VAN DE KOPPEL, *Self-organized patchiness and catastrophic shifts in ecosystems*, Science 305 (2004), pp. 1926–1929.
- [32] M. RIETKERK AND J. VAN DE KOPPEL, *Regular pattern formation in real ecosystems*, Trends Ecol. Evolu., 23 (2008), pp. 169–175.

- [33] L. A. D. RODRIGUES, D. C. MISTRO, AND S. PETROVSKII, *Pattern formation, long-term transients, and the Turing-Hopf bifurcation in a space- and time-discrete predator-prey system*, Bull. Math. Biol., 73 (2011), pp. 1812–1840.
- [34] A. ROVINSKY AND M. MENZINGER, *Interaction of Turing and Hopf bifurcations in chemical systems*, Phys. Rev. A, 46 (1992), pp. 6315–6322.
- [35] J. A. SHERRATT, *Pattern solutions of the Klausmeier model for banded vegetation in semi-arid environments I*, Nonlinearity, 23 (2010), pp. 2657–2675.
- [36] J. A. SHERRATT, *Pattern solutions of the Klausmeier model for banded vegetation in semi-arid environments II: patterns with the largest possible propagation speeds*, Proc. R. Soc. Lond. A, 467 (2011), pp. 3272–3294.
- [37] J. A. SHERRATT, *Pattern solutions of the Klausmeier model for banded vegetation in semi-arid environments V, the transition from patterns to desert*, SIAM J. Appl. Math., 73 (2013), pp. 1347–1367.
- [38] J. A. SHERRATT, *Periodic travelling waves in integrodifferential equations for nonlocal dispersa*, SIAM J. Appl. Dyn. Syst., 13 (2014), pp. 1517–1541.
- [39] J. A. SHERRATT, *Using wavelength and slope to infer the historical origin of semi-arid vegetation bands*, Proc. Natl. Acad. Sci. USA 112 (2015), pp. 4202–4207.
- [40] M. SCHEFFER, S. R. CARPENTER, T. M. LENTON, J. BASCOMPTE, W. BROCK, V. DAKOS, J. VAN DE KOPPEL, I. VAN DE LEEMPUT, S. LEVIN, E. H. VAN NES, M. PASCUAL, AND J. VANDERMEER, *Anticipating critical transitions*, Science 338 (2012), pp. 344–348.
- [41] J. A. SHERRATT AND G. J. LORD, *Nonlinear dynamics and pattern bifurcations in a model for vegetation stripes in semi-arid environments*, Theor. Popn. Biol., 71 (2007), pp. 1–11.
- [42] J. A. SHERRATT AND J. J. MACKENZIE, *How does tidal flow affect pattern formation in mussel beds? J. Theor. Biol.* 406 (2016), pp. 83–92.
- [43] H. B. SHI AND S. G. RUAN, *Spatial, temporal and spatiotemporal patterns of diffusive predator-prey models with mutual interference*, IMA J. Appl. Math., (2015), <https://doi.org/10.1093/imamat/hxv006>.
- [44] Y. L. SONG AND X. S. TANG, *Stability, steady-state bifurcations, and Turing patterns in a predator-prey model with herd behavior and prey-taxis*, Stud. Appl. Math. (2017), <https://doi.org/10.1111/sapm.12165>.
- [45] Y. L. SONG AND X. F. ZOU, *Bifurcation analysis of a diffusive ratio-dependent predator-prey model*, Nonlinear Dyn., 78 (2014), pp. 49–70.
- [46] Y. L. SONG AND X. F. ZOU, *Spatiotemporal dynamics in a diffusive ratio-dependent predator-prey model near a Hopf-Turing bifurcation point*, Comput. Math. Appl., 67 (2014), pp. 1978–1997.
- [47] Y. L. SONG, T. H. ZHANG, AND Y. H. PENG, *Turing-Hopf bifurcation in the reaction-diffusion equations and applications*, Commun. Nonlinear Sci. Numer. Simul., 33 (2016), pp. 229–258.
- [48] A. M. TURING, *The chemical basis of morphogenesis*, Phil. Trans. R. Soc. Lond., B237 (1952), pp. 37–72.
- [49] J. VAN DE KOPPEL, J. C. GASCOIGNE, G. THERAULAZ, M. RIETKERK, W. M. MOOIJ, AND P. M. J. HERMAN, *Experimental evidence for spatial self-organization in mussel bed ecosystems*, Science, 322 (2008), pp. 739–742.
- [50] J. VAN DE KOPPEL, M. RIETKERK, N. DANKERS, AND P. M. J. HERMAN, *Scale-dependent feedback and regular spatial Patterns in Young Mussel Beds*, Amer. Naturalist, 165 (2005), pp. 66–77.
- [51] W. M. WANG, Y. L. CAI, M. J. WU, K. F. WANG, AND Z. Q. LI, *Complex dynamics of a reaction-diffusion epidemic model*, Nonlinear Anal. RWA, 13 (2012), pp. 2240–2258.
- [52] R. H. WANG, Q. X. LIU, G. Q. SUN, Z. JIN, AND J. VAN DE KOPPEL, *Nonlinear dynamic and pattern bifurcations in a model for spatial patterns in young mussel beds*, J. R. Soc. Interface, 6 (2009), pp. 705–718.
- [53] J. F. WANG, J. P. SHI, AND J. J. WEI, *Dynamics and pattern formation in a diffusive predator-prey system with strong Allee effect in prey*, J. Differential Equations, 251 (2011), pp. 1276–1304.
- [54] R. Z. YANG AND J. J. WEI, *Stability and bifurcation analysis of a diffusive prey-predator system in Holling type III with a prey refuge*, Nonlinear Dyn., 79 (2015), pp. 631–646.
- [55] F. Q. YI, J. J. WEI, AND J. P. SHI, *Diffusion-driven instability and bifurcation in the Lengyel-Epstein system*, Nonlinear Anal. RWA., 9 (2008), pp. 1038–1051.
- [56] F. Q. YI, J. J. WEI, AND J. P. SHI, *Bifurcation and spatio-temporal patterns in a homogeneous diffusive predator-prey system*, J. Differential Equations, 246 (2009), pp. 1944–1977.

- [57] S. L. YUAN, C. Q. XU, AND T. H. ZHANG, *Spatial dynamics in a predator-prey model with herd behavior*, *Chaos*, 23 (2013), 0331023.
- [58] J. F. ZHANG, W. T. LI, AND X. P. YAN, *Hopf bifurcation and Turing instability in spatial homogeneous and inhomogeneous predator-prey models*, *Appl. Math. Comput.*, 218 (2011), pp. 1883–1893.
- [59] T. H. ZHANG, Y. P. XING, H. ZANG, AND M. A. HAN, *Spatio-temporal dynamics of a reaction-diffusion system for a predator-prey model with hyperbolic mortality*, *Nonlinear Dyn.*, 78 (2014), pp. 265–277.
- [60] H. Y. ZHAO, X. X. HUANG, AND X. B. ZHANG, *Turing instability and pattern formation of neural networks with reaction-diffusion terms*, *Nonlinear Dyn.*, 76 (2014), pp. 115–124.
- [61] W. J. ZUO AND J. J. WEI, *Multiple bifurcations and spatiotemporal patterns for a coupled two-cell Brusselator model*, *Dyn. Partial Differential Equations*, 8 (2011), pp. 363–384.
- [62] L. F. YANG AND I. R. EPSTEIN, *Oscillatory Turing patterns in reaction-diffusion systems with two coupled layers*, *Phys. Rev. Lett.*, 90 (2003), pp. 178–303.
- [63] L. F. YANG, A. M. ZHABOTINSKY, AND I. R. EPSTEIN, *Stable squares and other oscillatory Turing patterns in a reaction-diffusion model*, *Phys. Rev. Lett.*, 92 (2004), pp. 198–303.